DESIGN AND DEVELOPMENT OF A FLAPPING WING MECHANISM

PROJECT REPORT

Submitted by

ANUKUL NARAYAN R	**CB.EN.U4AEE09007**
SABARI GIRISH S	**CB.EN.U4AEE09042**
SARATH M R	**CB.EN.U4AEE09046**
VARUN ANANTHAKRISHNAN	**CB.EN.U4AEE09055**

In partial fulfillment for the award of the degree

Of

BACHELOR OF TECHNOLOGY

IN

AEROSPACE ENGINEERING

AMRITA SCHOOL OF ENGINEERING, COIMBATORE

AMRITA VISHWA VIDYAPEETHAM

COIMBATORE-641112

MAY 2013

AMRITA VISHWA VIDYAPEETHAM

(Faculty of Engineering)

AMRITA SCHOOL OF ENGINEERING, COIMBATORE-641112

BONAFIDE CERTIFICATE

This is to certify that the project entitled **DESIGN AND DEVELOPMENT OF A FLAPPING WING MECHANISM** submitted by **ANUKUL NARAYAN R. (CB.EN.U4AEE09007), SABARI GIRISH S. (CB.EN.U4AEE09042), SARATH M. R. (CB.EN.U4AEE09046), VARUN ANANTHAKRISHNAN (CB.EN.U4AEE09055)** in partial fulfillment of the requirement for the award of **Degree of Bachelor of Technology** in **Aerospace Engineering** is a bonafide record of the work carried out under my guidance and supervision at Amrita School of Engineering, Ettimadai.

SIGNATURE

Mr. T. Rajesh Senthil Kumar

Project Guide

Assistant Professor

Department of Aerospace Engineering

This report was examined and the candidates underwent Viva-Voce on:

Internal Examiner External Examiner

AMRITA VISHWA VIDYAPEETHAM

AMRITA SCHOOL OF ENGINEERING, COIMBATORE-641112

DEPARTMENT OF AEROSPACE ENGINEERING

DECLARATION

We, **Anukul Narayan R. (CB.EN.U4AEE09007), Sabari Girish S. (CB.EN.U4AEE09042), Sarath M. R. (CB.EN.U4AEE09046), Varun Ananthakrishnan (CB.EN.U4AEE09055)** hereby declare that this project report, entitled "**DESIGN AND DEVELOPMENT OF A FLAPPING WING MECHANISM"** is a record of original work done by us under the guidance of Mr. T. Rajesh Senthil Kumar, Assistant Professor, Department of Aerospace Engineering, Amrita School of Engineering, Coimbatore and that this work has not formed the basis for the award of any degree/ diploma/associateship/fellowship or a similar award, to any candidate in any university, to the best of our knowledge.

Place: Ettimadai

Date:

Anukul Narayan R.

Sabari Girish S.

Sarath M. R.

Varun Ananthakrishnan

COUNTERSIGNED

Dr. J. Chandrasekhar

Professor & Chairman

Department of Aerospace Engineering

ACKNOWLEDGEMENT

Firstly, we would like to thank our guide Assistant Professor **T. Rajesh Senthil Kumar** for guiding us throughout the course of this project and providing relentless support.

We would like to thank **Dr. J. Chandrasekhar**, Professor and Chairman, Department of Aerospace Engineering, Amrita School of Engineering, Ettimadai, Coimbatore for his ideas and suggestions.

We also express our gratitude to the Mechanical Lab faculty members for patiently allowing us to use their instruments for fabrication, the Organic Chemistry Lab faculty for permitting us to use their equipment for measurements and our Aerospace Lab faculty members **Mr. Girish** and **Mr. Sri Prasad** for providing us with facilities, instruments and support.

ABSTRACT

A flapping wing aircraft or ornithopter is a device that flies by flapping its wings. The flapping motion seeks to imitate the flight of birds or insects found in nature. Ornithopters offer practical benefits such as improved efficiency and manoeuverability compared to aircrafts. Miniature ornithopters are involved in surveillance. Ornithopters come in different shapes and sizes and can be manned or unmanned, powered by various sources such as rubber bands, steam, compressed air, human muscle power, electric power, engines etc. This project is limited to the study of the simple rubber band powered ornithopters.

This project was focused on the development of a miniature ornithopter model, using a rubber band as the power source and evaluating the performance parameters of the model. The potential energy of the rubber band is used to actuate the model. The potential energy is converted to kinetic energy by a crank mechanism. Three different types of rubber-bands were used for propelling the model: a conventional rubber band, a light rubber band and a heavy rubber band. A set of experiments were conducted to determine the angular frequency (which in turn was connected to power delivering capacity) of the three rubber bands. Based on this, an optimum rubber band (the light rubber band type) was selected. A suitable mechanism for the flapping wing was then developed based on the modification of conventional four bar mechanism.

In order to study the aerodynamic performance of the model, a set of experiments were conducted to evaluate the parameters such as the wing flapping frequency, with the help "Canon T3i Rebel" camera. The unsteady aerodynamic performance parameters such as the average lift & thrust, propulsive efficiency of the model were predicated theoretically by modified strip theory. Then, the effects of altering the tail angle of the ornithopter and its consequences have also been observed. Multiple models were fabricated with different wing and tail materials and their effects were observed.

TABLE OF CONTENTS

LIST OF FIGURES

LIST OF TABLES

LIST OF SYMBOLS AND ACRONYMS

S.No	Symbol	Description	Units
1	AR	Wing aspect ratio	-
2	C	Airfoil chord	m
3	$(C(k))_{jones}$	Finite wing Theodersen function	-
4	C'(k)	Theodersen function	-
5	$(C_d)_f$	Drag coefficient due to friction	-
6	C_{mac}	Coefficient of moment about aerodynamic center	-
7	$C_n(y)$	Section's unsteady lift coefficient	-
8	k	Reduced frequency	-
9	$\bar{L}$	Average lift	N
10	L(t)	Whole wing's instantaneous lift	N
11	$\overline{Pin}$	Average input power, throughout the cycle	Watt
12	$\overline{Pout}$	Average power output, throughout the cycle	Watt
13	Pin(t)	Instantaneous input power	Watt
14	Rn	Instantaneous Reynold's number	-
15	T	Instantaneous thrust	N
16	$\bar{T}$	Average thrust	N
17	T(t)	Whole wing's instantaneous thrust	N
18	U	Free stream velocity	m/s
19	V	Instantaneous velocity	m/s
20	V_n	Mid chord normal velocity due to wing motion	m/s

21	V_x	Instantaneous velocity in the x-direction	m/s
22	V_y	Instantaneous velocity in the y-direction	m/s
23	w_0	Downwash velocity	m/s
24	Y	Chord wise location	m
25	dD_{camber}	Chord wise force due to camber	N
26	dD_f	Sectional force due to viscosity	N
27	dF_x	Sectional x-direction force	N
28	dL	Segment's instantaneous lift	N
29	dM_a	Moment due to apparent mass and inertia	Nm
30	dM_{ac}	Sectional moment about aerodynamic center	Nm
31	dN	The section's total attached normal force	N
32	$(dN)_{sep}$	Total sectional force	N
33	dN_a	An apparent mass effect which acts at one-half chord position and normal to the chord	N
34	$(dNa)_{sep}$	Apparent mass effect which is found to be half the value dN_a	N
35	dN_c	A circulatory normal force normal to the chord acting at one-fourth chord location	N
36	$(dN_c)_{sep}$	Sectional circulatory normal force in the separated flow	N
37	dP_{in}	Instantaneous power required to move the section for attached flow	Watt
38	dT	Segment's instantaneous thrust	N
39	dT_s	A chord wise leading edge suction force	N
40	H	Plunging displacement	m
41	α_0	Zero lift angle of attack	rad

42	α'	Relative angle of attack at one-fourth chord location	rad
43	β_0	Amplitude of dynamic twist	rad
44	Γ	Section's instantaneous dihedral	rad
45	Γ_0	Maximum flapping angle	rad
46	$\delta\theta$	The dynamic twist(dynamically varying pitch angle	rad
47	$\bar{\eta}$	Average propulsive efficiency	-
48	η_s	The efficiency that accounts for the fact that most aerofoils due to friction	-
49	θ	Total twist	rad
50	θ'	$d\theta/dt$	rad/sec
51	θ_a	Flapping axis pitching up angle	rad
52	θ_w	The mean pitching angle of the chord with respect to flapping axis	rad
53	ρ	Density of air	kg/m^3
54	ω	Angular frequency of the flapping motion	rad/sec
55	ω'	Angular frequency of rubber band	rad/sec
56	$\dot{v}$	Time rate of change of the mid chord normal velocity	m/s^2

CHAPTER 1

INTRODUCTION

1.1 BACKGROUND

From time immemorial, man has been inspired and fascinated by the flight of birds and has wanted a place in the sky. Engineering always tries to replicate nature; hence when humans tried to create flying machines by mimicking the flight of birds, the flapping wing aircraft idea was developed naturally.

Flapping wing aircrafts are also known as Ornithopters. An ornithopter (In Greek *ornithos* means "bird" and *pteron* means "wing") [1] is an aircraft that flies by flapping its wings. The flapping motion seeks to imitate the flight of birds or insects found in nature. Ornithopters are classified into 2 types: manned or unmanned. Manned ornithopters may be powered by engines or powered by the muscles of the pilot. Unmanned ornithopters may be powered by rubber band, steam, compressed air, engines or electric power.

An ornithopters wing is made up of a thin membrane, which forms a curved shape when it is pushed against the air. The wings are connected to the body and follow an up and down pattern of motion. The up and down motion is less near the body compared to that near the wing tips.

The correct angle of attack has to be maintained throughout the wingspan while flapping. Since the part of the wing away from the body moves up and down more steeply than the part of the wing near the body, the wing has to twist in order to maintain the correct angle of attack. Due to the flexible wing material, this twisting is automatically done. As the wing moves down, the lift is produced in the forward direction in the part of the wing away from the body. Therefore the aircraft produces thrust during the downstroke.

In the upstroke, the part of the wing away from the body is angled in such a way that the angle of attack is reduced in order to provide least air resistance. Since the force produced during a stroke depends on the angle of attack, the upstroke produces lesser lift than the downstroke and as a result, the body will oscillate up and down slightly as the ornithopter flies. Therefore we infer that the part of the wing close to the body provides the lift and the part of the wing away from the body provides the thrust.


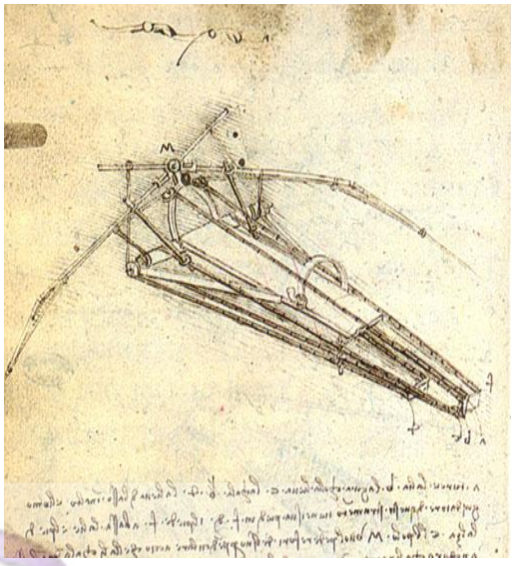

Fig 1.1: A picture of the Pushpaka Vimana [1] and Da Vinci's Ornithopter sketch [1]

The first evidence of an ornithopter comes from the Sanskrit epic the Ramayana, which describes an ancient flapping wing aircraft called the Pushpaka Vimana. One of the first pioneers in the western world for the development of flapping wing aircrafts was Leonardo Da Vinci, who sketched a human powered ornithopter model. The first ornithopters that achieved a successful flight were constructed in France. Gustave Trouvé and Pierre Jullien flew the first successful ornithopter, in the 18th century. Adalbert Schmidt and Alexander Lippisch flew the first manned engine-powered ornithopters in the 19th century. A human-powered ornithopter named Snowbird was flown by a team from the University of Toronto Institute for Aerospace Studies in 2010.

Ornithopters are important because they offer many practical benefits. Flapping wings provide improved efficiency, manoeuverability and even lesser noise compared to helicopters and propeller driven aircrafts. Miniature ornithopters can be used for surveillance and some ornithopters that resemble birds can be used to keep birds away from airports.

1.2 HISTORY OF ORNITHOPTERS

4th Century BC

The Pushpaka Vimana[1] from the Sanskrit epic Ramayana is the first description of an ornithopter.

In the Sanskrit epic Mahabharata, it is mentioned that the Asura Maya had a Vimana measuring twelve cubits in circumference, with four strong wheels. [2]

1485

Leonardo da Vinci sketched an unmanned ornithopter model that had membranous wings and worked by means of hand levers, pulleys and foot pedals. [1]

1858

An ornithopter model constructed by Pierre Jullien in France flew for about forty feet.[3]

1870

A model constructed by Gustave Trouvé, powered by gunpowder charges flew a distance of 70 metres during a demonstration for the French Academy of Sciences. [1]

Rubber band powered models were created by Alphonse Pénaud, Abel Hureau de Villeneuve, and Victor Tatin during the same period. [1]

1884

Lawrence Hargrave built multiple models of ornithopters which were powered by rubber bands, springs, steam, or compressed air. [4]

1894

Otto Lilienthal, famous for successful glider flights, constructed an ornithopter, but its development was incomplete due to his untimely death. [1]

1900

An internal combustion powered manned ornithopter was constructed by E.P. Frost.[5]

1930

A series of internal combustion powered ornithopters were flown by Alexander Lippisch and the NSFK in Germany. [6]

During the same period, Erich von Holst created an ornithopter with a bending wing, which was rubber band powered. [6]

1942

A longer flight of human-powered ornithopter was achieved by Adalbert Schmid at Munich-Laim, where it travelled a distance of 900 metres maintaining a height of 20 metres.[7]

1959

A human powered ornithopter was built by Emil Hartman which was capable of powered glides, but required the force of another towing vehicle in order to take off. [8]

1960

Percival Spencer, of the United States, developed a series of engine-powered free-flight ornithopter models. These were made in various sizes, with different engine sizes.[9]

1991

Jeremy Harris and James DeLaurier flew the first successful engine-powered remotely piloted ornithopter in Toronto, Canada. [9]

1999

A piloted ornithopter based on the Harris/DeLaurier design flew, which was capable of taking off from level pavement.[10]

2000

Aerovironment and Caltech developed the MicroBat, which was the first micro-sized ornithopter. [11]

2002

In Sweden a flapping wing robot that learned flight techniques was built by Krister Wolff and Peter Nordin of Chalmers University of Technology. [12]

An ornithopter constructed like a helicopter was developed by Prof. Theo van Holten. The device was called the ornicopter and it was made by constructing the main rotor so that it would have no reaction torque. [13]

2005

A human-muscle powered flight with flapping wing, created by Yves Rousseau was flown in his 212th attempt for a distance of 64 metres, observed by officials of the Aero Club de France. He was awarded the Paul Tissandier Diploma, awarded by the FAI for contributions to the field of aviation. [14]

2006

Delft University of Technology and Wageningen University developed the Delfly which could transition between hovering and forward flight. The Delfly has a small camera, which transmits live images to a computer on the ground; hence it has the capacity for autonomous navigation. Later, the Delfly II and the Delfly micro were made by the Delft University. [11]

A team headed by Professor James DeLaurier at the University of Toronto Institute for Aerospace Studies, had flown an engine-powered piloted ornithopter at the Bombardier Airfield at Toronto called the UTIAS Ornithopter No.1. The ornithopter made a jet assisted take-off and flew for about 14 seconds. [15]

2007

Petter Muren constructed a radio-controlled ornithopter that has a wingspan of 10 cm and weighs 1 gram. It is currently the world's smallest radio-controlled ornithopter. [11]

2008

Falconer Robert Musters designed a real looking mechanical hawk which was used in Schiphol Airportto scare away birds that could damage the engines of airplanes. [16]

2010

A human-powered ornithopter named Snowbird was piloted by Todd Reichert from the University of Toronto Institute for Aerospace Studies. The ornithopter was capable of self-powered flight once aloft.[17]

2011

AeroVironment, Inc. announced a remotely piloted ornithopter resembling a large hummingbird for possible spy missions. [11]

A robotic flapping wing aircraft called the SmartBird based on the motion of a seagull, was introduced by the engineers at the Festo Bionic Learning Network in March 2011.[18]

1.2.1 CURRENT

2013

IIT Kanpur is actively involved in development of flapping wing Micro Air Vehicles through DRDO sponsored projects. Several prototypes have been constructed and tested in wind tunnel for loads measurement. A theoretical aerodynamic model has been developed to predict the loads generated by flapping wing vehicle, which has been used in optimization of wing twist. [19]

1.2.2 FUTURE

In the future miniature ornithopters can be used for surveillance by military organizations for scouting areas in close range without being detected. Manned ornithopters, may be produced on a large scale, to be used for commercial transport because they are more manoeuverable and energy-efficient than airplanes. Hybrid ornithopters [20] can also be made, by implementing features of aircrafts like jet engines and propellers.

1.3 LITERATURE REVIEW

Tanakon Tantanvat and Sridhar Kota [21] studied about power flow in compliant mechanisms employed for dynamic applications. Through their studies they proposed a compliant flapping mechanism which can reduce the input power requirement by 10% when compared to that of four bar flapping mechanism using springs.

Vance A. Tucker [22] explains about the effect of variable wing span for gliding bird flight. Through his studies, he calculates the aerodynamic forces and thereby aerodynamic performance of the bird during its flight.

C. J. Pennycuick [23] studied about the control of gliding angle by the Rüppell's Griffon Vulture (*Gyps rueppellii*). He speaks about the different ways in which the Vulture uses its legs and neck to increase/decrease the gliding angle by altering the drag contributed by the legs and neck.

C. J. Pennycuick [24] developed an empirical relation between wing beat frequency to mass of the bird, wing area, wing span and air density by studying 32 morphologically

different species representing 18 different families and mass ranging from 20g to 5kg. The wing beat frequency is then used to find the wing wavelength and the ratio of wing wavelength to wing span.

B. G. Newman [25] studied about the soaring and gliding flight performance of the Black Vulture (*Coragyps atratus*). He finds that the bird is able to perform better by altering the wing span and geometry.

Karl Axel Strang [26] studied about the flapping flight of pterosaurs (Coloborhynchus robustus) as these were the most efficient flapping fliers and found out that they exploited their membrane wings in a sophisticated manner for the flight and he went on to develop a code to predict the aerodynamic parameters of the pterosaur.

Vance A. Tucker and G. Christian Parrott [27] performed studies on aerodynamics of gliding flight for the falcon and other birds and performed experiments in the wind tunnel and estimated the performance parameters of the birds during gliding.

Chao Wang, Chaoying Zhou et.al. [28] have performed optimization studies on single crank double rocker mechanism which was found to have many problems due to asymmetric flapping of left and right wing. They analysed the mechanism in ADAMS environment and have improved the design of the mechanism and reduced the asymmetry in flapping.

Thomas J. Mueller and James D. DeLaurier [29] addressed aerodynamic problems associated with designing a small aerial vehicle and came out with the effect of Reynolds number and Aspect Ratio on small aerial vehicle design including ornithopters.

Theodore Yaotsu Wu [30] studied about Fish Swimming and Insect/Bird flight and has developed a theoretical model for the above.

Jerke Eisma [31] conducted flow visualization experiments on the Delfly-II in order to understand more about the aerodynamics and used a six component force sensor to measure the forces on the Delfly-II in the forward flight configuration. Using these results, the design has been improved.

Yu-Chong Tai, Chih-Ming Ho et. al. [32] developed the first electrically powered palm-sized ornithopter and have briefly explained about the experiments and work done.

Lan Liu, Zongde Fang and Zhaoxia [33] have done optimization design on a flapping wing MAV which was found to pitch towards left or right or crash during flight. The characteristics of nervure position and biomimetic wings were also studied.

Dmytro Silin [34] studied about aerodynamics and flight performance of a flapping wing micro air vehicle and developed methods to predict its aerodynamic parameters.

Mark Ryan [35] has done optimization studies on compliant mechanisms for flapping wing MAV. The flapping mechanism was studied for better transmission of power and to lower the input power.

Harijono Djojodiharjoa [36], Alif Syamin Syazwan Ramli et.al. have done the kinematic and aerodynamic modelling of flapping wing ornithopter.

J. D. Delaurier [37] developed an aerodynamic model for flapping wind model which was used for our model to predict the lift, drag etc.

G. C. H. E de Croon, K M E de Clercq et.al. [38] studied the development of the Delfly - design wise, aerodynamic wise and vision based control wise by performing experiments and incorporating state of art equipments for vision.

Lung-Jieh Yang, Cheng Kuei Hsu et. al. [39] have done studies on figure of eight flapping induced by flexible wing motion, which was used for a comparison with our figure of eight.

Tay Wee Beng [40] studied the dynamics and control of an EPO (electric-powered prototype ornithopter). They studied factors affecting lift such as wing shape and material and designed 2 new wings namely the spring and camber wing to improve the EPO's performance.

1.4 SCOPE

The scope of the project is focussed towards the technological development in the flapping wing regime and indigenous and cost effective production of flapping wings in-house. It also emphasizes on the need for national security and civil surveillance.

1.5 AIM

The aim of this project is:

- To fabricate a simple rubber band powered ornithopter capable of flight.
- Selecting the optimum rubber band based on angular frequency.
- To analyse the crank mechanism used and determine various parameters such as wing flapping frequency, forward flight velocity etc.
- To determine the aerodynamic performance parameters of the ornithopter using modified strip theory for unsteady aerodynamics.

1.6 OUTLINE OF CHAPTERS

Chapter 2 explains the various problems encountered during fabrication and how multiple changes were implemented in design to obtain the final model.

Chapter 3 deals with the parametric analysis of crank mechanism, various tests and experiments performed with the model and rubber bands.

Chapter 4 deals with theoretical estimation of various aerodynamic performance parameters of the ornithopter using modified strip theory for unsteady aerodynamics.

CHAPTER 2

DEVELOPMENT OF THE SUCCESSFUL MODEL

2.1 BUILD 1

Building a rubber band model (RBM) was the first step that was taken. Several internet resources on how to build a RBM were studied in detail. Initial models were closely related to different designs from different sources. Almost all the models in the sources had the same wing span and maximum wing chord. Hence it was decided to maintain the wing span of 16 inches, a maximum chord of 5 inches and a semi elliptical planform, taking into consideration that several models which were flown successfully with this wing area and planform. Similarly the tail was fixed to be an equilateral triangle of side 7 inches. The first design was inspired by Instructables. [41]

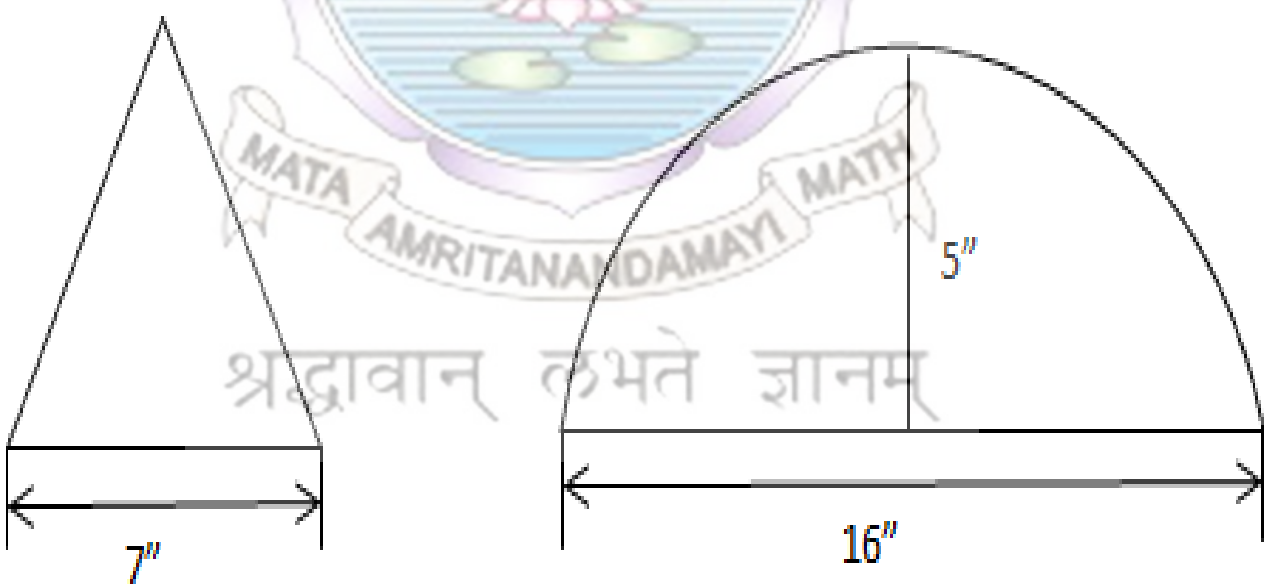

Fig 2.1: The Tail and Wing planform dimensions

Fig 2.2: The first model design

The model was made with ice cream sticks. Thin strips of sun-ban sheet were used as wing and tail spars. Cyano acrylate was used to stick the pieces together. A plastic bag material of thickness 0.03mm was used for the wing. A bead was used to reduce friction between the crank and the body during rotation. A conventional rubber band was used. Instead of a music wire, a 2.5 mm mild steel rod was used. This model was unable to fly.

The problem incurred was that the rubber band was not providing enough torque. Hence a heavy rubber band was used. It did flap after changing the rubber band, but it did not meet its goal. It was assumed that this might be because of the weight difference between balsa wood and ice cream sticks.

Another model of the same design was made using balsa wood and the same was used for wing spars and tail frame. For this model it was found that the strength of balsa wood was the problem. As the holes were drilled in the wood, there was a possibility that it would pierce in due to the softness of the wood and when the mild steel wire was put in and the rubber band was wound, the grains would fall apart leaving a hole open at the tail end or at the nose end and the whole assembly would collapse. Hence another design was necessary.

2.2 BUILD 2

The next design was developed from "Building an Ornithopter" by William Gurstelle [42]. In this design instead of using balsa, carbon fibre rods of 1mm diameter were used as wing spars and tail frame. A heavy rubber band was used in this case.

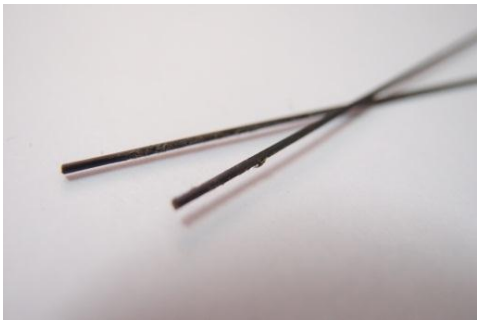

Fig 2.3: 1mm diameter carbon fibre rods

Here also, the strength of balsa was causing problems while winding the rubber band. At the tail end, the grains would fall apart opening up the hole and at the nose end it would break along the ply due to the pull of the rubber band when winded.

Slight modifications were implemented on the design in order to counter the weakness of balsa at different areas. As for the front it was decided to stack up small pieces of ice cream sticks and stick it at the bottom as a crank stand-off. This gave freedom to wind the rubber band more due to the increased buckling strength, but the model still did not meet the goal. When analysed it was found that there was no symmetry while the wings were flapping.

This might be either because of the use of rolled papers as pivoted points, which we could not make using the same paper as they mentioned and the substitute used was also not good enough to maintain the distance between the holes, which was not specified. Another problem would be in the crank.

Finally, maintaining the base design for the top pivot points, two rolls of insulation tape were made with a single layer of paper rolled in the inner most winding for smooth movement of the mild steel wire. The distance between the top pivot points and the bottom was arbitrarily fixed. The modified design is as shown below. A light weight, highly elastic rubber band was used for the model. This model was also unable to meet its goal.

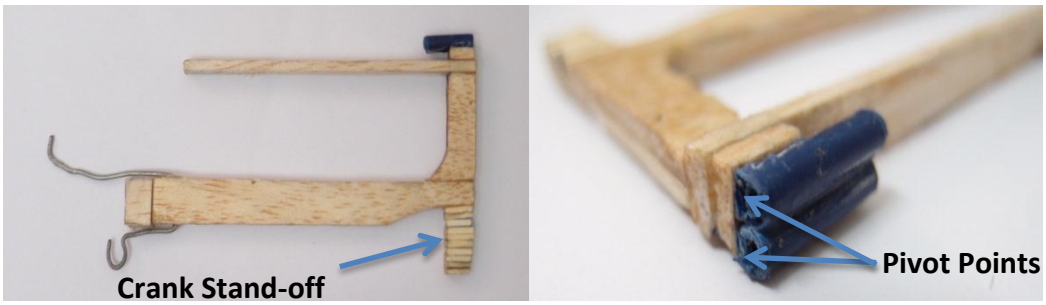

Fig 2.4: The second model design showing crank stand-off and pivot points

2.3 THE FINAL BUILD

The final design was inspired by that of Birdkit[43] with slight customizations.Even after these modifications there was slight delay between the two wings on flapping. This was fixed by modifying the crank design, which might have been necessary due to the change in the distance between the top and bottom holes. It was decided to bring the pivot points as close as possible and make it in a stack of ice cream sticks. Further a thinner 1mm diameter mild steel wire was used as the crank material. The modified crank details are given below. As a result the connecting rod's length was also modified for the smooth rotation of the crank.

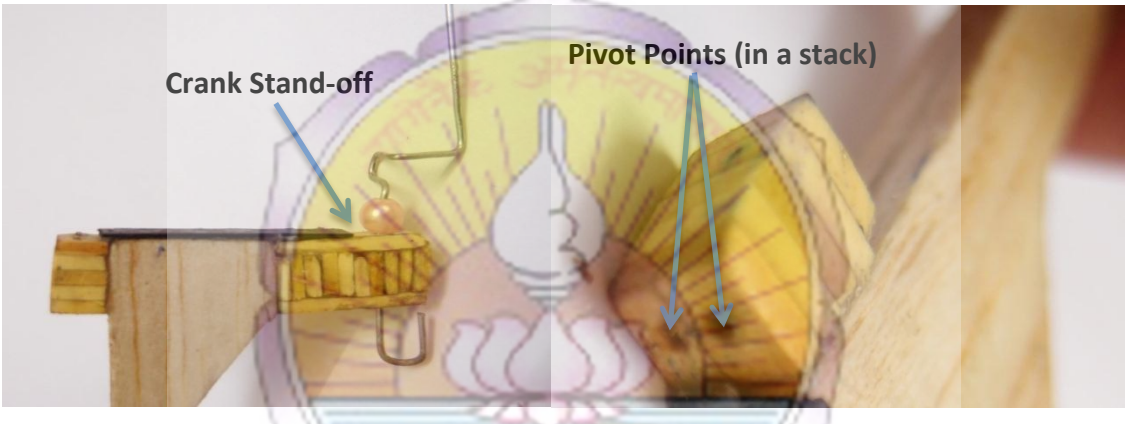

Fig 2.5: The modified design and pivot points in a stack of ice cream sticks

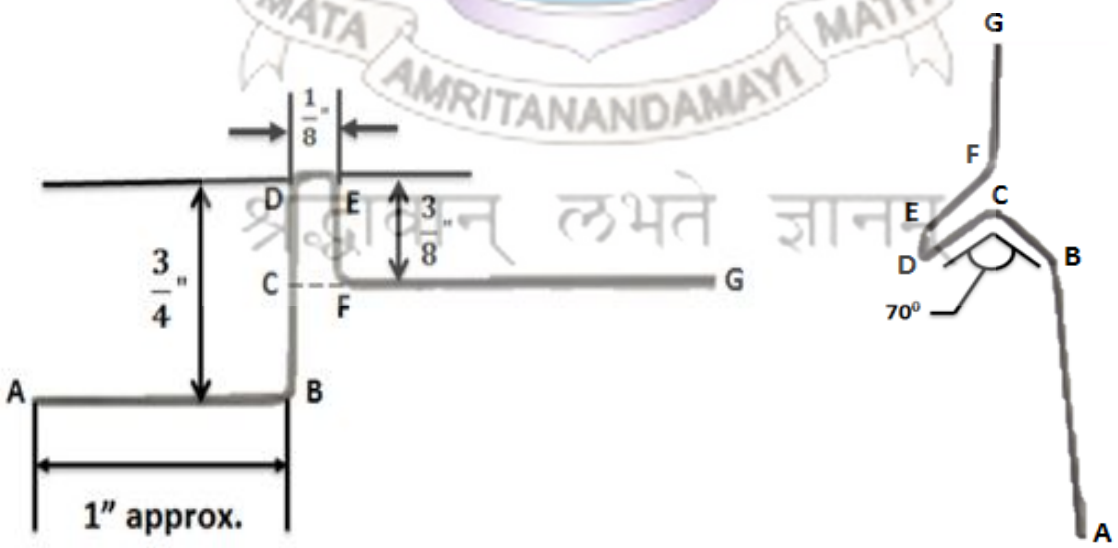

Fig 2.6: Modified crank dimensions

An efficient design to overcome the problems caused due to the softness of balsa at the tail end was developed. The tail design is as shown below. The breaking of the balsa along the ply at the nose end was fixed by sticking two strips of carbon fibre plates of length 35mm width 3mm and thickness 0.5mm.which was a self-proposed idea to prevent the crack initiation.

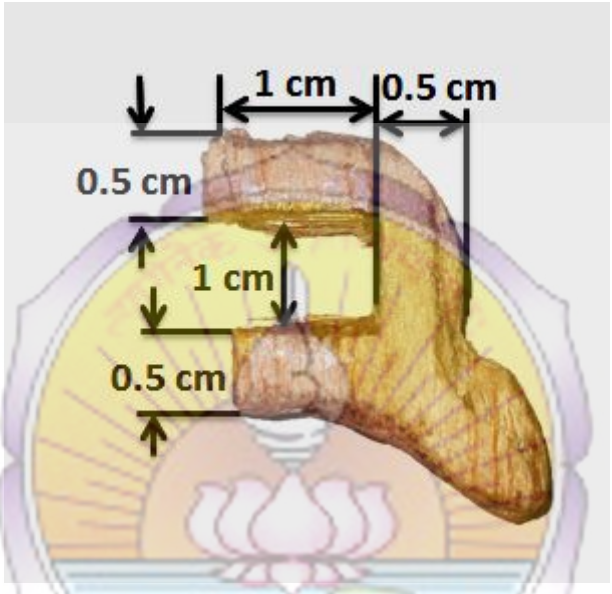

Fig 2.7: Modified tail end

Fig 2.8: The model before and after the breaking of balsa along the ply at the nose end

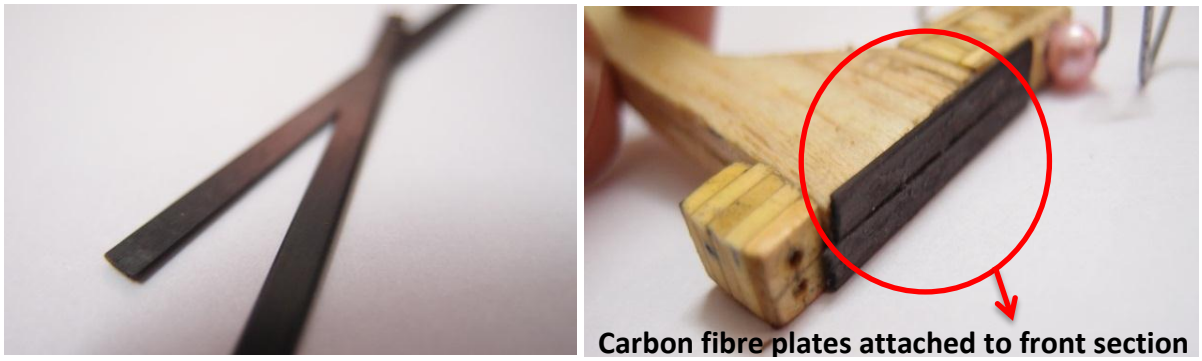

Fig 2.9: The carbon fibre plates and the modified frontal section of the model with carbon fibre

When the tail was fixed to the mild steel wire, the tail was found to rotate about wire. Hence, a new wire design was created to hold the tail fixed at a desired angle. It was decided to use napkin of thickness 0.12 mm as wing and tail material and the rubber band used was a light weight, highly elastic rubber band. The final overall design specifications are depicted in the following figure. The model was flown successfully for about 10 seconds in the first trial and many more followed. The model was named **KAVAS-I.T3.**

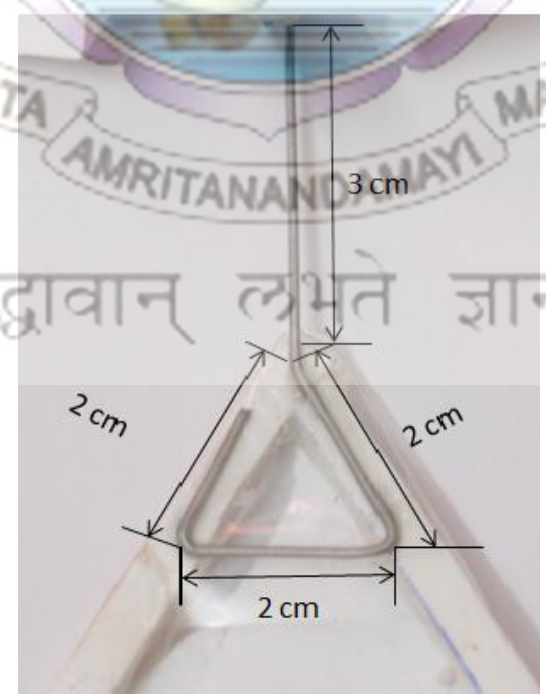

Fig 2.10: Tail wire design

Fig 2.11: Wing and tail material (napkins)

Fig 2.12: Light rubber band (highly elastic) used for the model

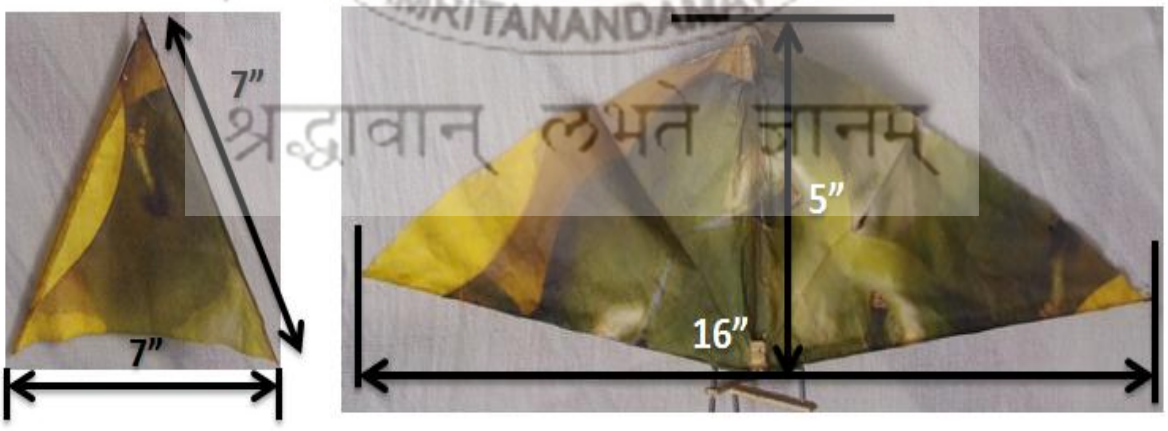

Fig 2.13: Dimensions of the wing and tail of the final design

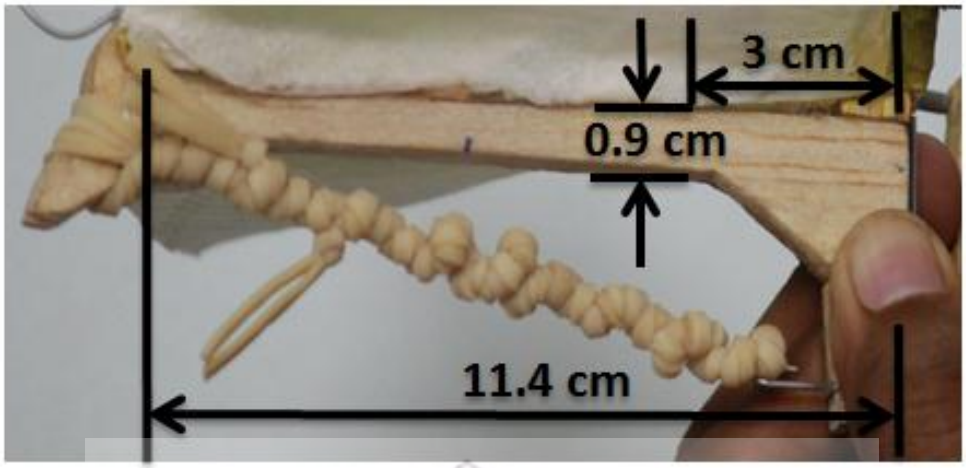

Fig 2.14: Fuselage dimensions of the successful model

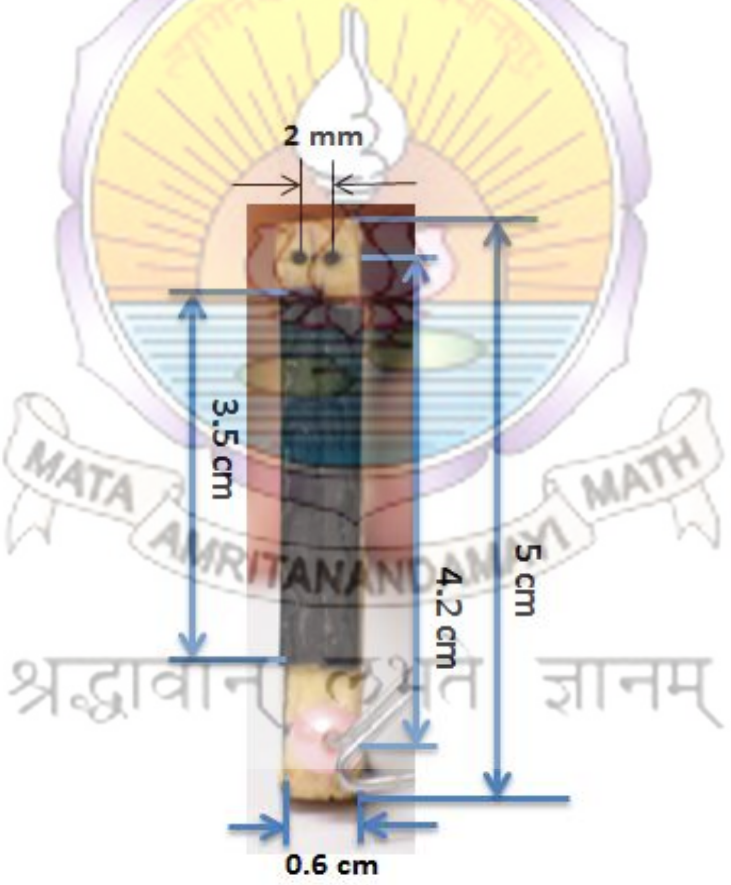

Fig 2.15: Frontal dimensions of the successful model

Fig 2.16: A snapshot of the successful flight and various views of KAVAS-I.T3

This model was studied in detail starting with the engineering analysis of the crank. An experiment was devised to analyze the characteristics of different rubber bands. With the help of a camera – the Canon T3i Rebel, photographic techniques were used to find the flapping frequency and to prove that the wings of the model also follow a figure of '8' path while flapping, which is in accordance with the nature. The forward velocity was estimated by experiments and the effect of tail angle was observed. Further aerodynamic forces such as lift, drag of the model were determined theoretically.

CHAPTER 3

EXPERIMENTAL ANALYSIS

3.1 PARAMETRIC ANALYSIS OF CRANK MECHANISM

From the successful model a parametric study of the crank mechanism was done to find the flapping frequency in terms of the rubber band input frequency. Each wing along with the connecting rod and the crank can be treated as a 4 bar mechanism, so we have two 4 bar mechanisms, equivalent to the 2 wings and crank motion. The dimensions including lengths and angles were measured for three different wing positions, namely the top, bottom and mean position of the wing (during flapping) and analysis is done for these three positions.

Velocity and acceleration analysis was done for the three positions. The two fixed points can be joined to form a stationary bar and the other 3 moving bars, together with it form the 4 bar linkage. Assuming the rubber band to have a constant angular velocity, the crank has only radial acceleration and the same procedure is followed to get the acceleration diagrams for three different positions. For a body in circular motion, angular velocity is similar to angular frequency, as their magnitudes are numerically equivalent in case of circular motion [44]. For the mean position we get two diagrams, as it occurs twice in a cycle, one while flapping up and other while flapping down. The results obtained from both mean positions were similar. The velocity diagrams are as given below:

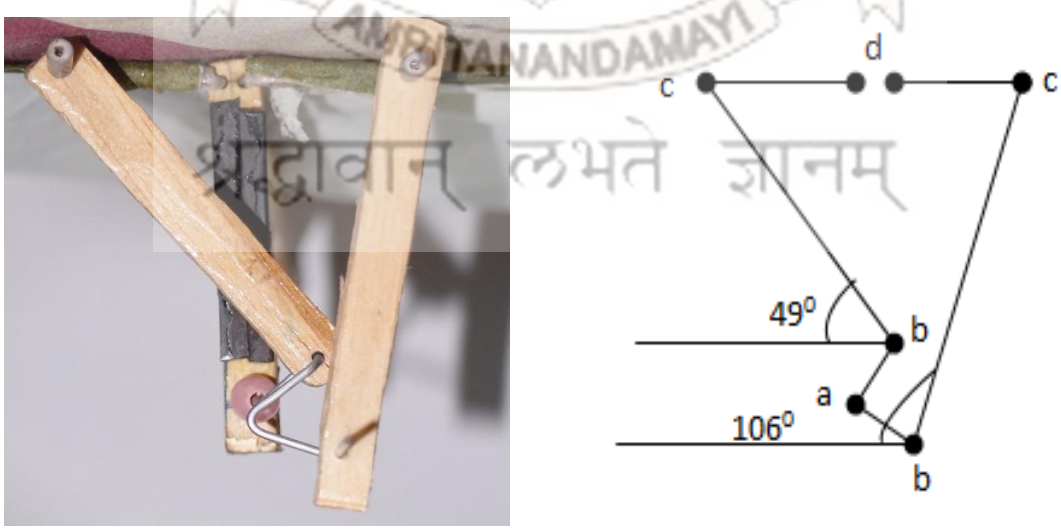

Fig 3.1: The first mean position of the crank and a diagrammatic representation of the crank

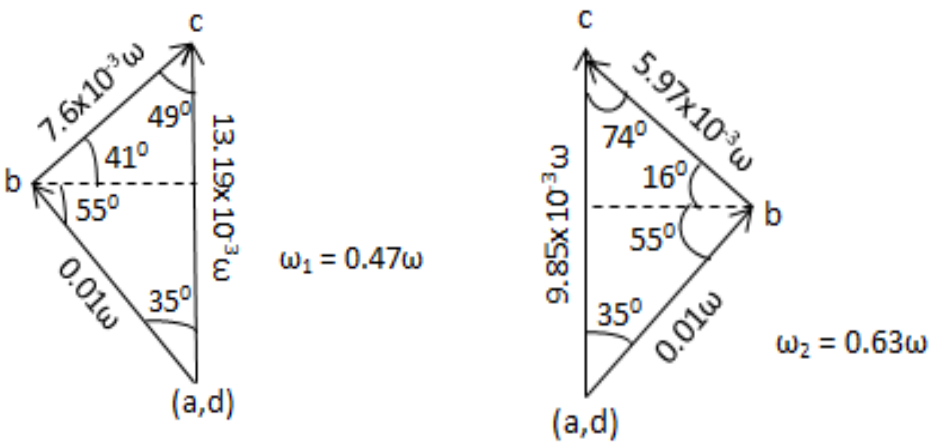

Fig 3.2: Velocity diagrams of the first mean crank position

Fig 3.3: The second mean position of the crank, and a diagrammatic representation of the crank

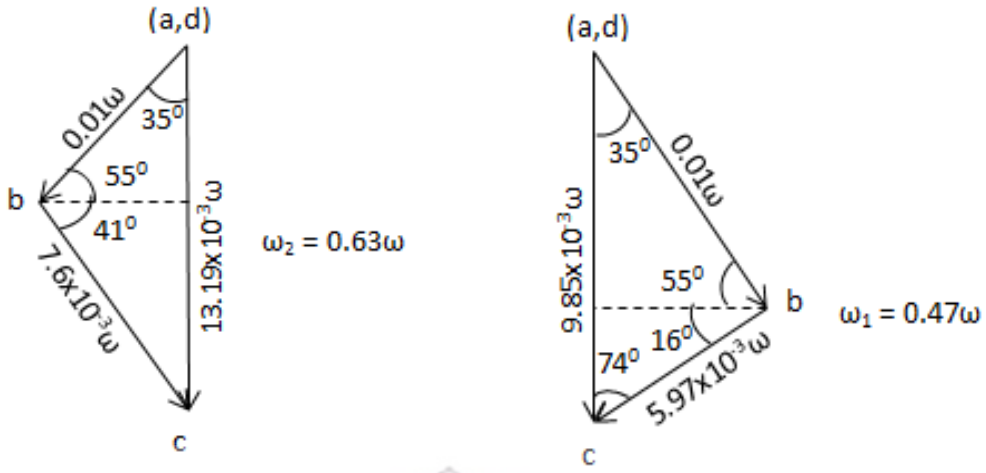

Fig 3.4: Velocity diagrams of the second mean crank position

From the analysis, the relation between crank angular frequency and flapping angular frequency was obtained. At the two extreme points the wings come to rest, hence the angular frequency is zero. By considering the mean wing case, while using the relation between the two angular frequencies obtained from the analysis, the corresponding rubber band frequency is found.

The two angular frequencies are related by,

$\omega = 0.55\ \omega'$ (average 'ω' of the two mean positions).

By experimentally determining the flapping frequency of the wing, a refinement of the crank analysis was done later.

3.2 EXPERIMENT TO DETERMINE RUBBER BAND BASED ON ANGULAR FREQUENCY

An experiment was done to find the frequency and the resilience of different rubber bands. The experimental setup used was a plastic container with hooks at the two ends as shown in figure 3.6. The distance between the two hooks is in such a way that the rubber band will be stretched in the same length as it will be in the model. The hook on the top has an extension that comes out of the container as a pointer. The pointer is also used to rotate the top hook while the bottom hook remains fixed. This gives us a similar situation that is seen while winding the rubber band in the actual RBM. This pointer, when released after winding, will rotate in the opposite direction, unwinding the rubber band inside the container. This

happens in fractions of seconds and is hard to clock it using a timer. Hence the motion of the pointer, when released is recorded using a camera – the Olympus XZ1 and the time is calculated using a video editing software called Sony Vegas Pro 11 in which the time in milliseconds can be observed. Three different rubber bands were tested namely: TYPE 'A' – normal commercially available rubber bands, used in sets of 5; TYPE 'B' – Heavy rubber bands and TYPE 'C' – lightweight highly elastic rubber bands.

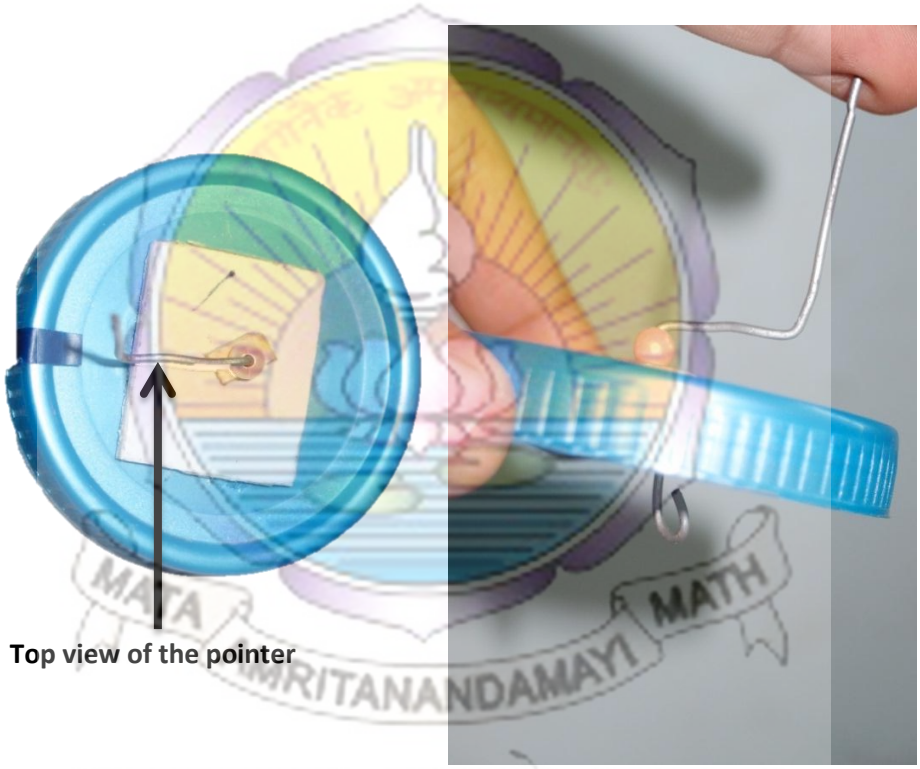

Fig 3.5: The top view and side view of the container lid showing the pointer and hook

Fig 3.6: The fixed hook at the bottom of the container and a rubber band placed in the container

Fig 3.7: The experimental setup for rubber band selection

Fig 3.8: Conventional rubber band

Fig 3.9: Heavy rubber band

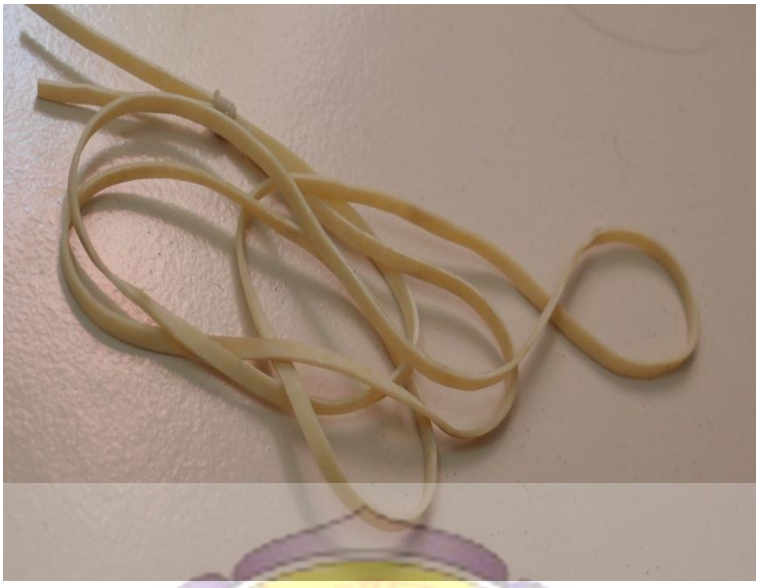

Fig 3.10: Light rubber band

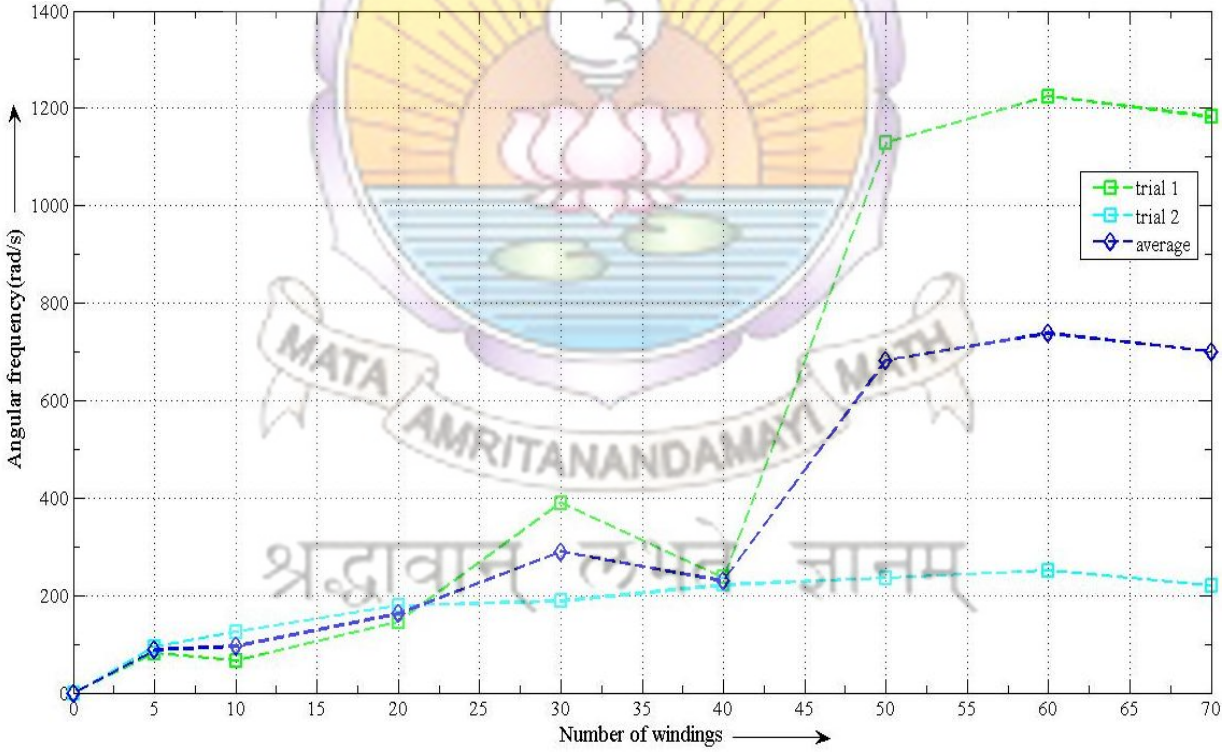

Fig 3.11: Angular frequency vs. number of windings for a conventional rubber band

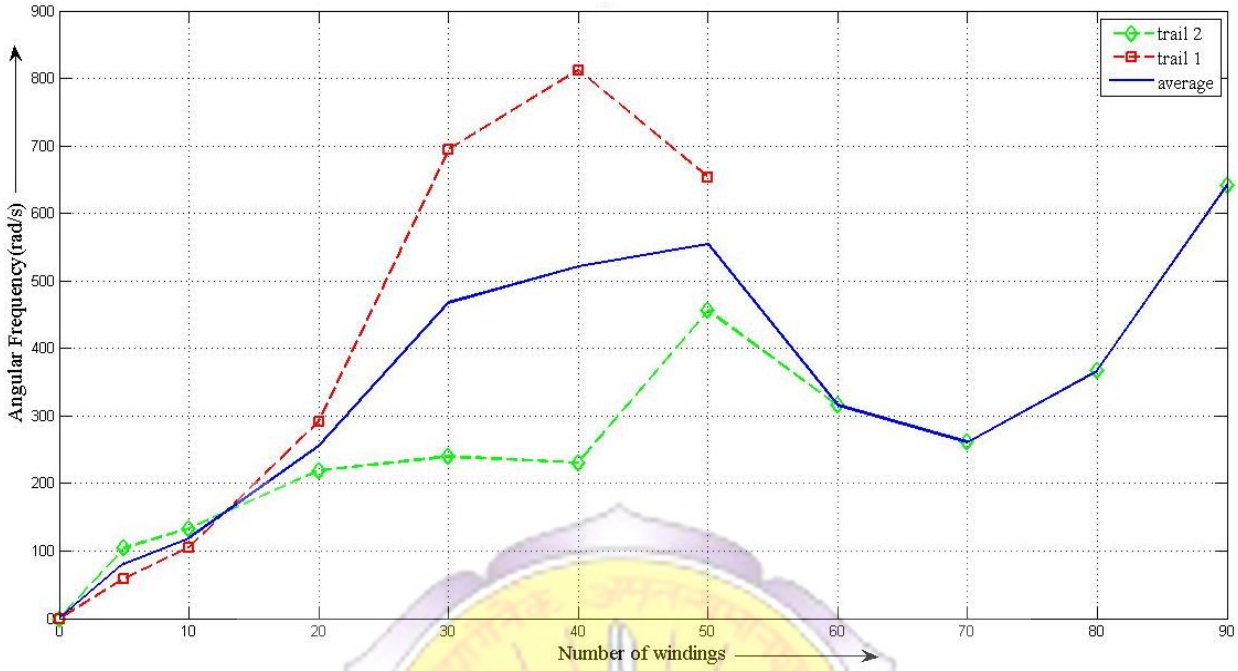

Fig 3.12: Angular frequency vs. number of windings for a heavy rubber band

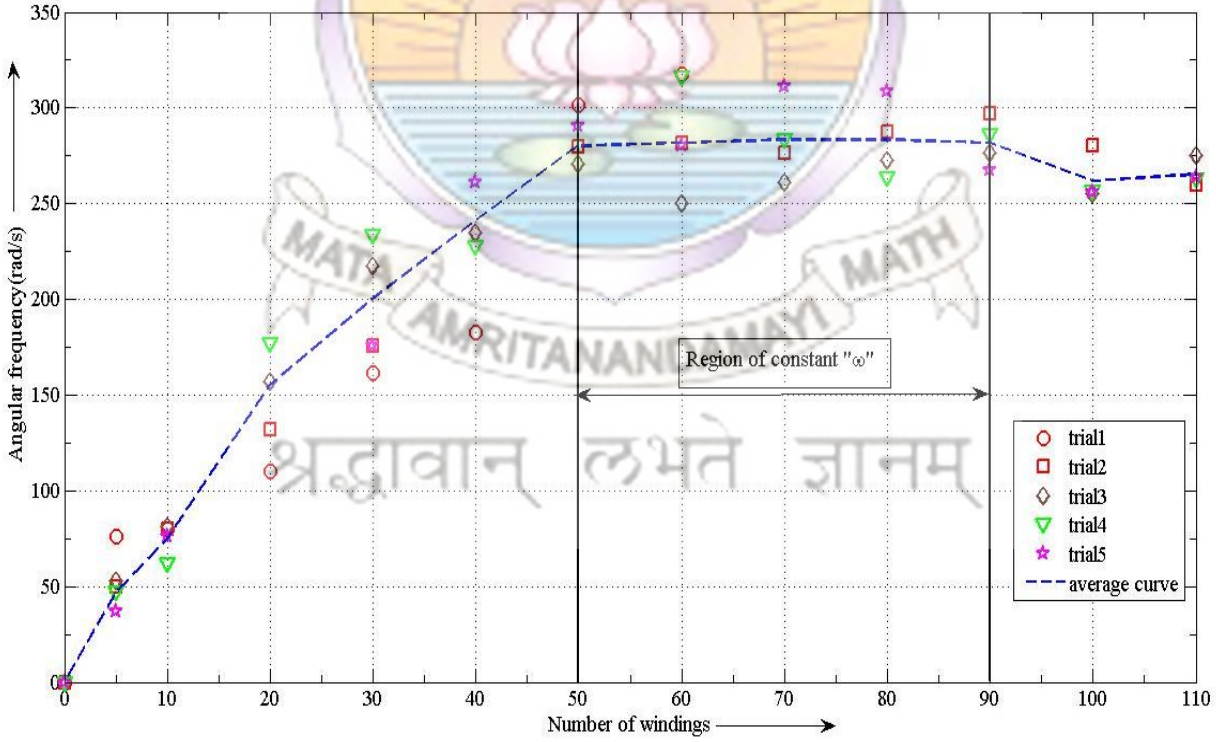

Fig 3.13: Angular frequency vs. number of windings for a light rubber band

From the above graphs it was observed that the TYPE C rubber bands were consistent and has a higher resilience when compared to the other types. Hence it was decided to use a TYPE C rubber band for the model.

3.3 DETERMINING THE WING FLAPPING FREQUENCY

Frequency is the number of cycles or oscillations in one second. Keeping this in mind the flapping frequency was found using photographic techniques. This experiment is inspired by a genre of photography called light painting in which the exposure time is increased and a light source is moved in the frame. The end result will be photo with the path traced by the light source during the exposure time.

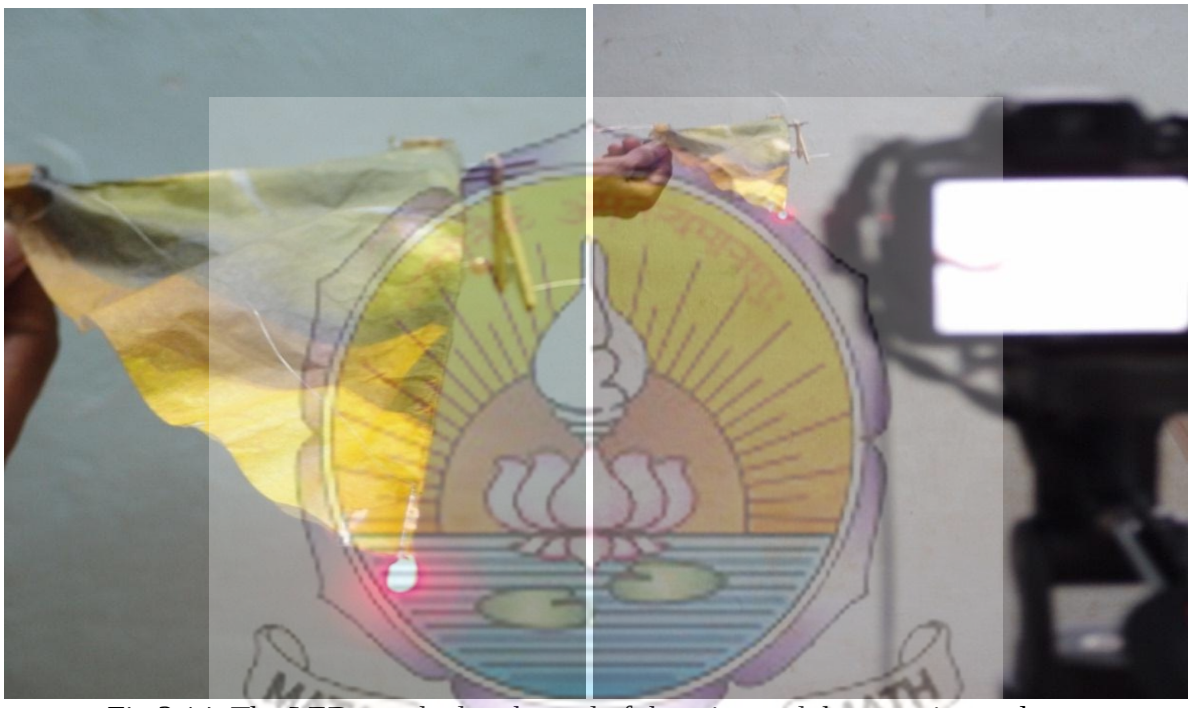

Fig 3.14: The LED attached at the end of the wing and the experimental setup

In this experiment the exposure time was fixed for one second and a LED is fixed at the tip of the spar of one wing. The body of the model was held by hand and moved forward while it flaps during the exposure time, so that it does not retrace its path on the frame. The end result is the number of cycles the wing completes in one second which can be manually counted from the photograph. Shown below are the trials performed for the same number of windings in the same model. From the trials, the average flapping frequency was found to be **6.15 Hz.**

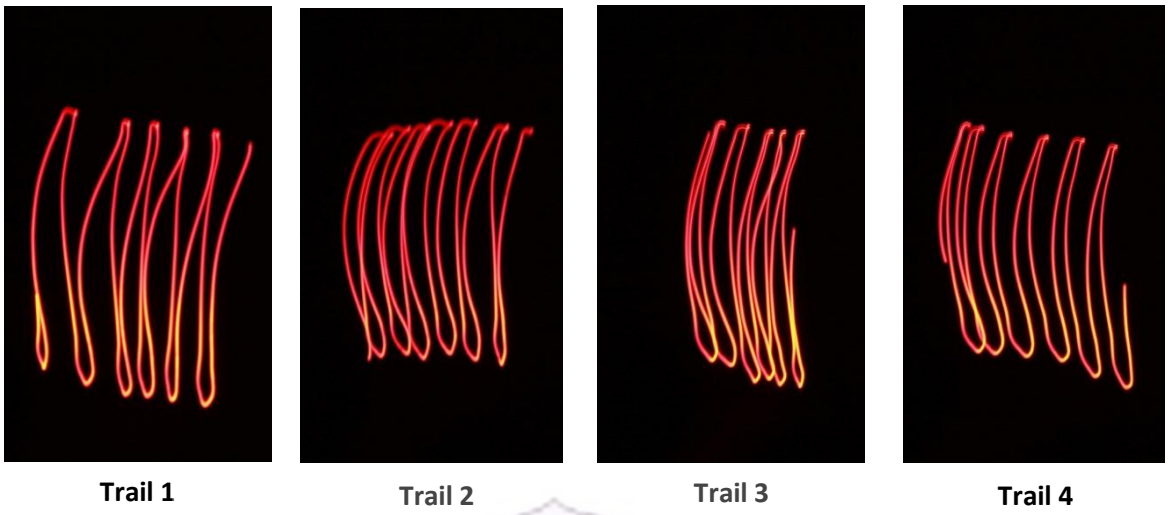

Fig 3.15: Trials obtained from the experiment.

From various trials conducted, the frequency (average) obtained was 6.15Hz for 50 windings of the rubber band. Using this data a refinement of the crank analysis was done.

Hence, $\omega = 2\pi f = 38.64$ rad /sec

The 'ω' from the experiment was 38.64. The rubber band's angular frequency is 70.26, but from the experiments conducted on the light rubber band for free rotation, we get an angular frequency of 280 for 50 windings.

$$\frac{((280)-(70.26))}{280} = 0.75$$

This is the fraction of energy which is not obtained as output. This implies that only 25% of the input energy is obtained as the output. The rest of the energy is spent in the linkage motion and frictional losses.

3.4 UNFOLDING THE FIGURE OF '8'

An ornithopter is said to be able to fly if its wing follows a figure of '8' pattern in accordance with nature. To verify that the ornithopter follows the same pattern, we devised an experimental setup. The experiment was done using the same technique, except that this time there were 4 LED's fixed at different points as shown below and this time the model is held stationary while flapping. First, the path traced by all LED's was obtained and then the individual paths of each of the LED's are observed. The LED distances mentioned below are taken from the leading edge. Shown below are the experimental setup and the results obtained.

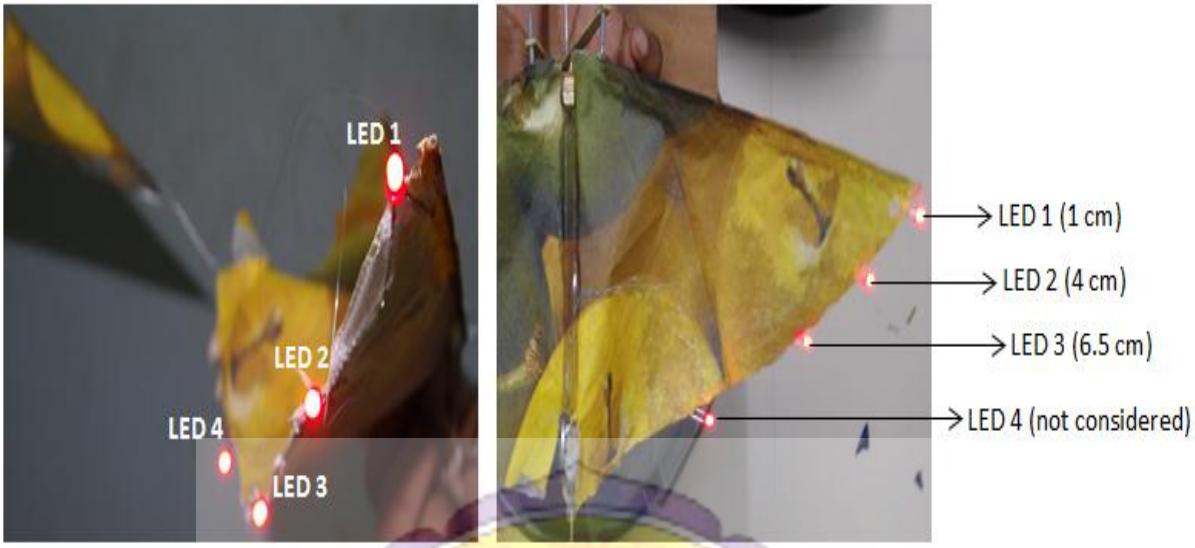

Fig 3.16: Locations of the LED's along the wing of the ornithopter

Fig 3.17: The experimental setup for the figure of '8'

Fig 3.18: The figure of '8' patterns obtained from the experiment

The complete figure of '8' was obtained from the 3rd LED (shown in figure 3.18), hence providing evidence for material flexibility and also satisfying the theoretical figure of '8' concept.

3.5 FORWARD VELOCITY ESTIMATION

The velocity of the model was estimated as follows:

- The model was released from an elevated position and the distance covered by the model was measured with a rope and the time taken was obtained from the camera.

- The height from which the model was released was also measured.

- With the above values, the hypotenuse was calculated taking the horizontal and vertical distances and the final distance value is calculated.

- The distance value calculated from the hypotenuse is divided by the time interval to calculate the forward velocity. The average velocity of the model was found to be **2.808 m/s.** Given below are the forward velocity values obtained from the experiment:

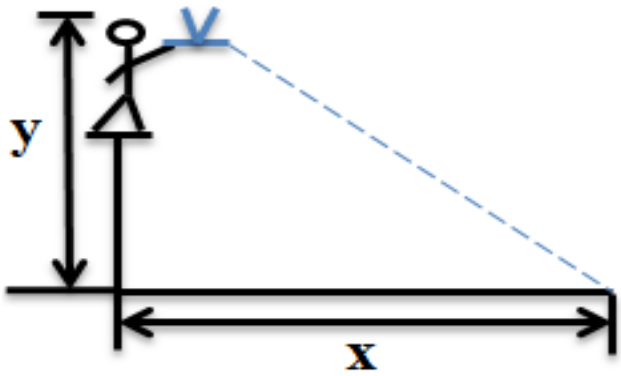

Fig 3.19: Representation of forward velocity estimation

Table 1: Velocity table for a tail angle of 20^{o} and 30 rubber band windings

S.No.	'X' Distance (m)	'Y' Distance (m)	Hypotenuse (m)	Time (s)	Velocity (m/s)
1	3.3	2.6	4.20	1.535	2.74
2	3.3	2.7	4.26	1.468	2.90
3	3.3	2.55	4.17	1.634	2.55
4	3.3	2.55	4.17	1.501	2.78
5	3.3	2.6	4.20	1.368	3.07

3.6 EFFECT OF TAIL

In order to study the effect of tail orientation on the flight path, the tail angle of the model was altered and the consequences were observed. The following figures show the various tail angles that were experimented with.

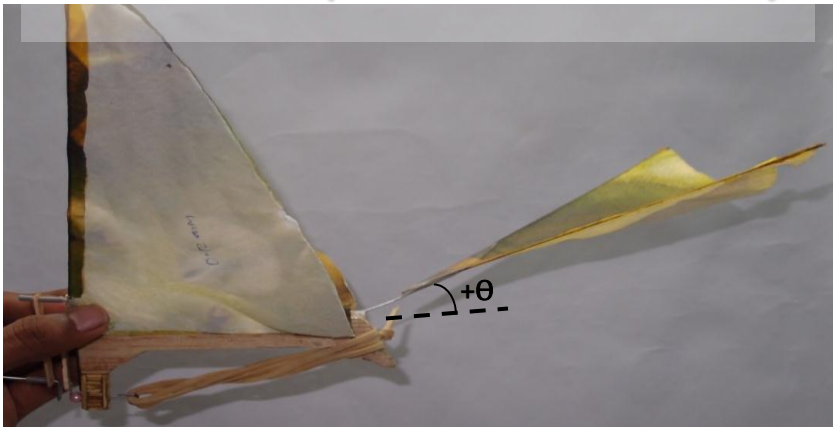

Fig 3.20: Positive tail angle

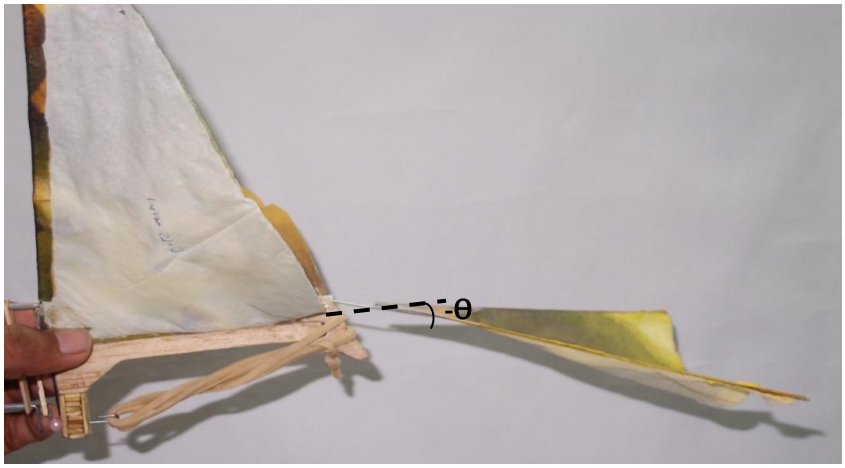

Fig 3.21: Negative tail angle

Fig 3.22: Zero tail angle

It was observed that:

- For a positive tail angle, the ornithopter climbs.
- For a zero degree angle, the ornithopter maintains its altitude and moves forward.
- For a negative tail angle, the ornithopter dives.

Thus we can infer that for a successful flight we would require a positive tail angle.

3.7 MODELS BUILT

It was decided to study the effect of materials on the flight of the ornithopter. Hence, many models were made with different wing and tail materials.

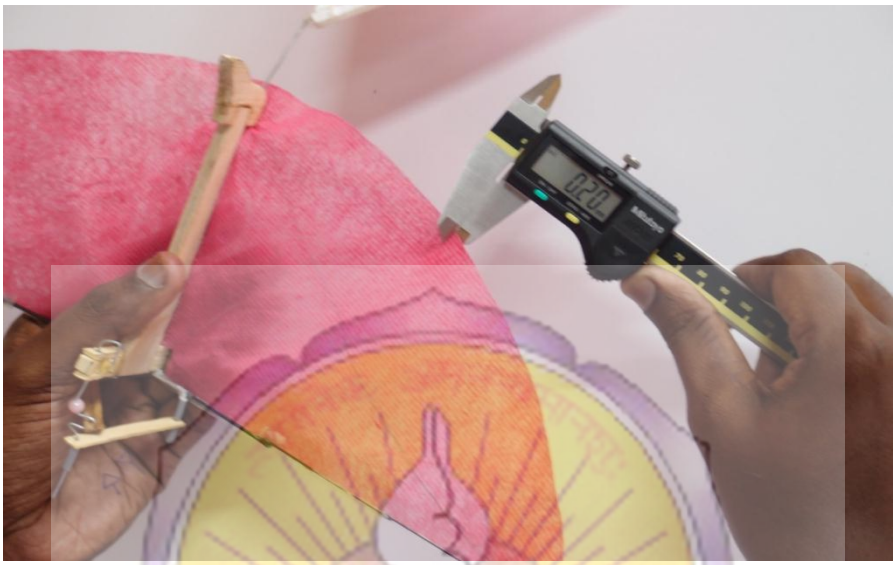

Fig 3.23: Digital Vernier Calliper used to measure material thickness

To measure the thickness of the wing materials, a digital vernier calliper was used which has a least count of 0.01mm. The weight of one square centimeter of the material was also measured using an electronic weighing machine, The Shimadzu AUW 220D, having a least count of 1 mg.

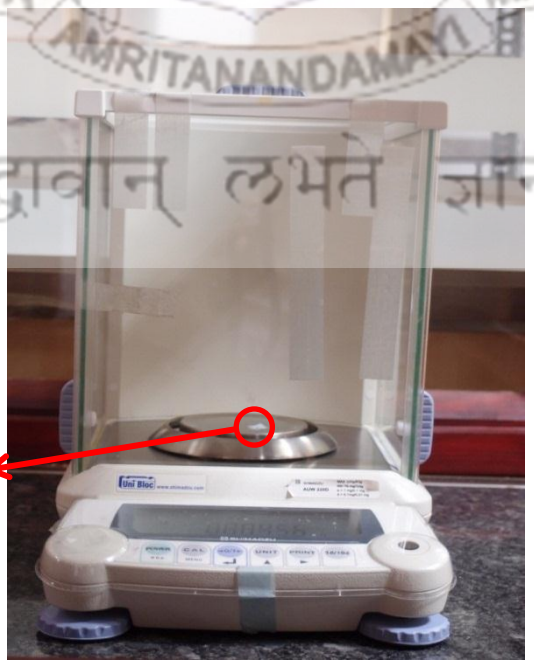

Fig 3.24: The electronic weighing machine used (Shimadzu AUW 220D)

Table 2: Classification of the properties of the materials used

S.No.	Model Name	Material Used	Material thickness(mm)	Material weight (g/cm^2)	Material Density(g/cm^3)
1	K-I.T3	Napkin	0.12	0.00508	0.4233
2	K-I.F	Fabric	0.20 - 0.23	0.00412	0.19162
3	K-I.PC	Polythene	0.05 - 0.06	0.00555	1.009
4	K-I.PT	Polythene	0.02 - 0.03	0.00245	0.98
5	K-I.PW	Polythene	0.04	0.00438	1.095
6	K-I.P	Paper	0.09	0.00880	0.977

It was observed that:

- The napkin model covered the longest distance.
- The paper model covered the least distance.

CHAPTER 4

AERODYNAMIC MODELLING OF THE ORNITHOPTER

The aerodynamic modelling of the ornithopter is required to predict the performance parameters and the variation of the lift and thrust with respect to various parameters. The aerodynamic modeling is done based on DeLaurier's modified strip theory [37]. In this the case the wing is divided into finite number of strips having equal span. Each strip is assumed to act as if it were part of elliptical wing planform of the same aspect ratio. The wing is assumed to be rigid, that is, it has no folding motion like that of a bird. The unsteady wake effects are accounted through modified theodersen function. The model has no camber, but partial leading edge suction effects are accounted. Post stall behaviour is also considered in the analysis.

4.1 DELAURIER'S MODEL

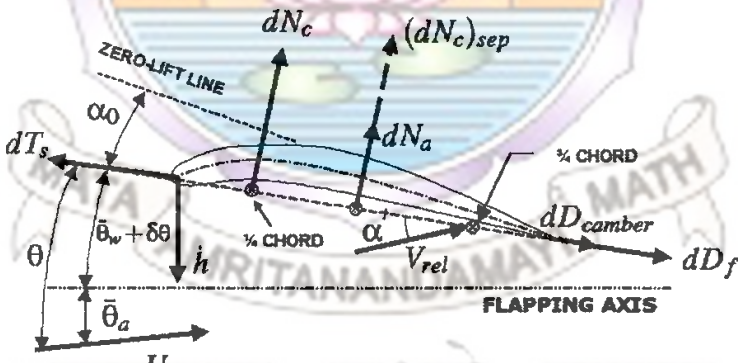

Fig 4.1: Wing's section showing the forces acting (photo courtesy: DeLaurier[37])

The ornithopter is assumed to be having flapping axis to be pitched up by an angle θ_a. The mean pitching angle of the chord wise with respect to flapping axis is θ_w. The sectional zero lift angle of attack is (α_0). The plunging displacement is given by

$$\Gamma = \Gamma_0 \cos(\omega t) \qquad (1)$$

$$h = -\Gamma_0 * y * \cos(\omega t) \qquad (2)$$

The dynamic twist (dynamically varying pitch angle) is

$$\delta\theta = -(\beta_0 y)\sin(\omega t) \quad (3)$$

The total twist is given by, $\theta = \delta\theta + \theta_a + \theta_w$ (4)

$$\bar{\theta} = \theta_a + \theta_w \quad (5)$$

The forces on each strip are determined by the instantaneous parameters. The section operates in stalled or unstalled regime which is determined by the relative angle of attack at the leading edge. In the unstalled regime of flight, the various forces acting are:

1. A circulatory normal force normal to the chord acting at one-fourth chord location.
2. An apparent mass effect which acts at one-half chord position and normal to the chord.
3. A chordwise leading edge suction force
4. A chordwise drag force due to the skin friction.
5. The chordwise force due to camber.

$$\alpha = \frac{((h\cos(\bar{\Theta} - \Theta a) + \frac{3}{4}c\dot{\Theta} + U(\Theta - \bar{\Theta}))}{U} \quad (6)$$

The section's unsteady lift coefficienct is given by

$$C_n(y) = 2\pi(\alpha' + \alpha_0 + \theta_a + \theta_w) \quad (7)$$

$$\alpha' = [\frac{AR * C'(k)}{2+AR}]\alpha - \frac{w0}{U} \quad (8)$$

Where k is the reduced frequency and is given by,

$$k = \frac{c*\omega}{2U} \quad (9)$$

The above equation is further simplified as

$$\alpha' = \frac{AR}{2+AR}(F'(k)\,\alpha + \frac{c}{2U}\frac{G'(k)}{k}\dot{\alpha}) - \frac{w0}{U} \quad (10)$$

$\frac{w0}{U}$ refers to the induced angle of attack and is given by,

$$\frac{w0}{U} = \frac{2(\alpha 0 + \bar{\theta})}{2+AR} \quad (11)$$

$$F'(k) = 1 - \frac{E*k}{k*k+Q*Q} \quad (12)$$

$$G'(k) = -\frac{E*Q}{k*k+Q*Q} \quad (13)$$

$$E = \frac{0.5AR}{2.32+AR} \quad (14)$$

$$Q = \frac{0.772}{AR}+0.181 \quad (15)$$

$$dN_c = \frac{\rho*U*V}{2}*C_n(y)*cdy \quad (16)$$

$$V = \sqrt{(Vx^2 + Vy^2)} \quad (17)$$

$$V_x = U\cos(\theta) - \dot{h}\sin(\theta - \theta_a) \quad (18)$$

$$V_y = U(\alpha' + \bar{\theta}) - 0.5*c*\dot{\theta} \quad (19)$$

The additional normal force due to the apparent mass effect is,

$$dN_a = \frac{\rho\pi c^2}{4}*\dot{v}dy \quad (20)$$

$$\dot{v} = U\dot{\alpha} - 0.25*c*\ddot{\theta} \quad (21)$$

Therfore, the section's total attached normal force is,

$$dN = dN_a + dN_c \quad (22)$$

The sharp diversion of flow around the leading edge causes the rapid change in the velocity and results in the leading edge suction force.

$$dT_s = \eta_s*\pi[\alpha' + \bar{\theta} - 0.25*c*\frac{\dot{\theta}}{U}]^2*\rho U*V*c*dy \quad (23)$$

The efficiency η_s accounts for the fact that most aerofoils due to friction will have less than 100% leading edge suction effect. The force due to viscosity is,

$$dD_f = (C_d)_f*\rho*V_x^2*c*dy/2 \quad (24)$$

$$(C_d)_f = \frac{0.89}{\log(Rn)^{2.58}} \quad (25)$$

The chordwise forces due to camber is given by,

$$dD_{camber} = -2\pi\alpha_0(\alpha' + \bar{\theta})*\frac{\rho*U*V}{2}*c*dy \quad (26)$$

$$dF_x = dT_s - dD_f - dD_{camber} \quad (27)$$

The dynamic stall condition for each section as given by Prouty[45],

$$\alpha_{stall} = (\alpha_{stall})_{static} + \varepsilon * [\frac{c*\dot{\alpha}}{2U}]^{0.5} \quad (28)$$

Therefore the condition for attached flow is given by,

$$(\alpha_{stall})_{min} \leq [\alpha' + \bar{\theta} - (\frac{3}{4}\frac{c*\dot{\theta}}{U})] \leq (\alpha_{stall})_{max} \quad (29)$$

In the stalled regime of flight, the various forces acting are:

1. The normal force to the chord
2. An apparent mass effect which is found to be half the value dN_a.
3. dT_s, dD_f = 0 (all the chordwise flows are negligible)

$$(dN_c)_{sep} = (C_d)_{cf} * \rho * \acute{V} * V_n * c * dy * 0.5 \quad (30)$$

Where,

$$\acute{V} = \sqrt{(Vx^2 + Vn^2)} \quad (31)$$

$$V_n = \dot{h}\cos(\theta - \theta_a) + 0.5*c*\dot{\theta} + U\sin(\theta) \quad (32)$$

$$(dN)_{sep} = (dN_c)_{sep} + (dN_a)_{sep} \quad (33)$$

Now the equations for segment's instantaneous lift and thrust are,

$$dL = dN\cos(\theta) + dF_x\sin(\theta) \quad (34)$$

$$dT = -dN\sin(\theta) + dF_x\cos(\theta) \quad (35)$$

This may be integrated along span to give the whole wing's instantaneous lift and thrust:

$$L(t) = 2\int_0^{\frac{b}{2}} cos\,(\Gamma) dL \quad (36)$$

$$T(t) = 2\int_0^{b/2} dT \quad (37)$$

The average lift and average thrust are expressed as:

$$\bar{L} = \frac{\omega}{2\pi}\int_0^{2\pi} L(\omega t)dt \quad (38)$$

$$\bar{T} = \frac{\omega}{2\pi}\int_0^{2\pi} T(\omega t)dt \quad (39)$$

The instantaneous power required to move the section for attached flow can be calculated as:

$dP_{in} = dF_x * \dot{h}\sin(\theta - \theta_a) + dN[(\dot{h}\cos(\theta - \theta_a) + 0.25*c\dot{\theta})] + 0.25*dN_a*c*\dot{\theta} - dM_a*\dot{\theta} - dM_{ac}*\dot{\theta}$ (40)

dM_a includes the apparent camber and the apparent-inertia moments and is given by

$$dM_a = -[\frac{1}{16}\rho\pi c^3\dot{\theta}U + \frac{1}{128}\rho\pi c^4\ddot{\theta}]dy \quad (41)$$

$$dM_{ac} = 0.5*\rho c^2 dy*C_{mac} \quad (42)$$

For separated flow, the input power expression becomes,

$$dP_{in} = (dN)_{sep}[\dot{h}\cos(\theta - \theta_a) + 0.5*c*\dot{\theta}] \quad (43)$$

The instantaneous aerodynamic power absorbed by the whole wing is found from,

$$P_{in}(t) = 2\int_0^{b/2} dPin \quad (44)$$

The average input power, throughout the cycle, is given by,

$$\overline{P_{IN}} = \frac{\omega}{2\pi}\int_0^{2\pi} Pin(t)dt \quad (45)$$

The average power output for the wing is given by,

$$\overline{Pout} = \bar{T}U \quad (46)$$

The average propulsive efficiency may be calculated as,

$$\bar{\eta} = \overline{Pout}/\overline{P_{IN}} \quad (47)$$

4.2 MODIFIED DELAURIER'S MODEL

In the DeLaurier's model the instantaneous height 'h' is taken as

$$h = -\Gamma_0*y*\cos(\omega t) \quad (2)$$

This is obtained by approximating $\sin\Phi = \Phi$. This approximation is valid for angles upto 15^0.

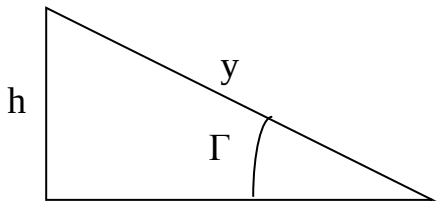

Fig 4.2: Right triangle for modified DeLaurier model

From the above triangle,

$$h = -y*\sin(\Gamma*\cos(\omega t)) \quad (48)$$

$$\dot{h} = \Gamma_0*y*\omega[\sin(\omega t)*\cos(\Gamma_0*\cos(\omega t)] \quad (49)$$

$$\ddot{h} = \Gamma_0*y*\omega^2[(\sin(\omega t)*\Gamma_0*\sin(\omega t)*\sin(\cos(\Gamma_0*\cos(\omega t)) + (\cos(\omega t)*\cos(\Gamma_0*\cos(\omega t)\ ] \quad (50)$$

Implementing this modification to the DeLaurier model, the aerodynamic modelling was done and the results were validated.

4.3 DE-LAURIER MODEL VALIDATION

In order to verify the accuracy associated with the code and the modified code, computational studies were performed on the pterosaur replica and the results obtained were compared with that of DeLaurier and Shyy et. al. [46].

The aerodynamic characteristics of the pterosaur, which were given as the input are:

$\alpha_0 = 0.5^\circ$

$\eta_s = 0.98$

$C_{mac} = 0.025$

$(\alpha_{stall})_{max} = 13^\circ$

Span =18ft

The wing is divided into 12 stations of width 9″ and the mid chord length of each station as shown in figure 4.3.

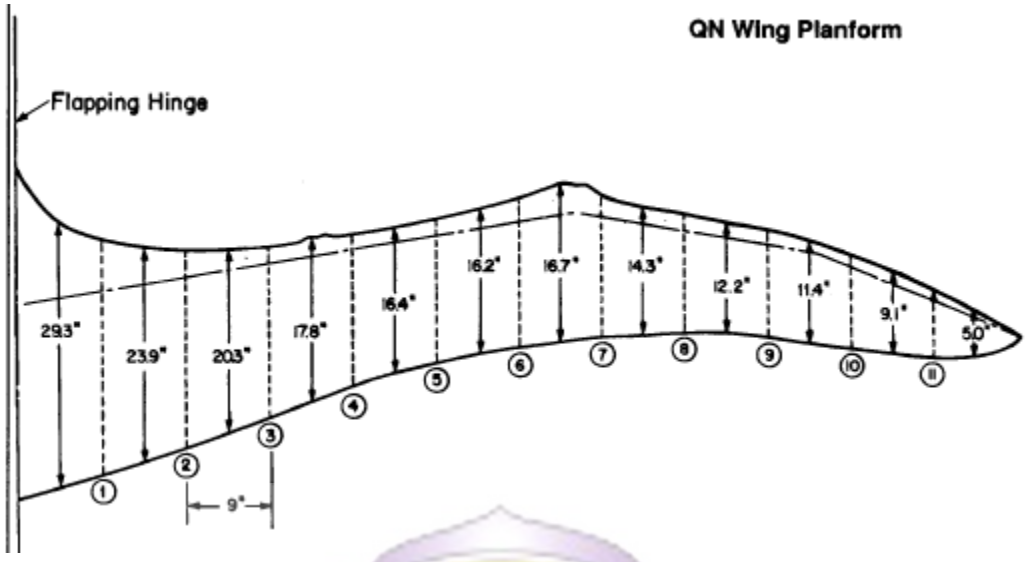

Fig 4.3: The Pterosaur wing planform [37]

Table 3: A comparison of results obtained from the Present model and Tay Wee Beng [40]

Model Used	**θ_a (deg)**	**Γ_0 (deg)**	**β_0 (deg/ft)**	**Lift (lb)**	**Thrust (lb)**	**Power (lbft/s)**	**Efficiency**
Present Model	7.2	16	1.75	42.2236	0.47604	92.8065	0.2708
Tay Wee Beng	7.2	16	1.75	40.0947	0.5424	89.7885	0.2658
Difference	-	-	-	2.1289	0.06636	3.018	0.005
Present Model	7.5	20	2.25	43.1162	1.2208	126.4369	0.3540
Tay Wee Beng	7.5	20	2.25	40.9423	1.1592	122.1982	0.4174
Difference	-	-	-	2.1739	0.0616	4.2387	0.0634
Present Model	7	40	4.75	37.1986	6.1647	335.2210	0.6743
Tay Wee Beng	7	40	4.75	35.3231	5.8539	322.8307	0.7979
Difference	-	-	-	1.8755	0.3108	12.3903	0.1236

Table 4: Results obtained from modified DeLaurier model

θ_a(deg)	**Γ_0 (deg)**	**β_0(deg/ft)**	**Lift(lb)**	**Thrust(lb)**	**Power(lbft/s)**	**Efficiency**
7.2	16	1.75	42.2172	0.5001	89.338	0.2463
7.5	20	2.25	43.0987	1.0513	118.2691	0.3911
7	40	4.75	36.9875	3.8510	228.958	0.6981

The slight variations in the values might be due to the improved version in the software used (MATLAB). From the modified approach it has been found that the maximum efficiency occurs at β_0 = 2.25deg/ft and the maximum efficiency is 0.4 it has also been found that the minimum θ_a required for satisfying lift = weight condition is 9deg and β_0 = 3deg/cm.

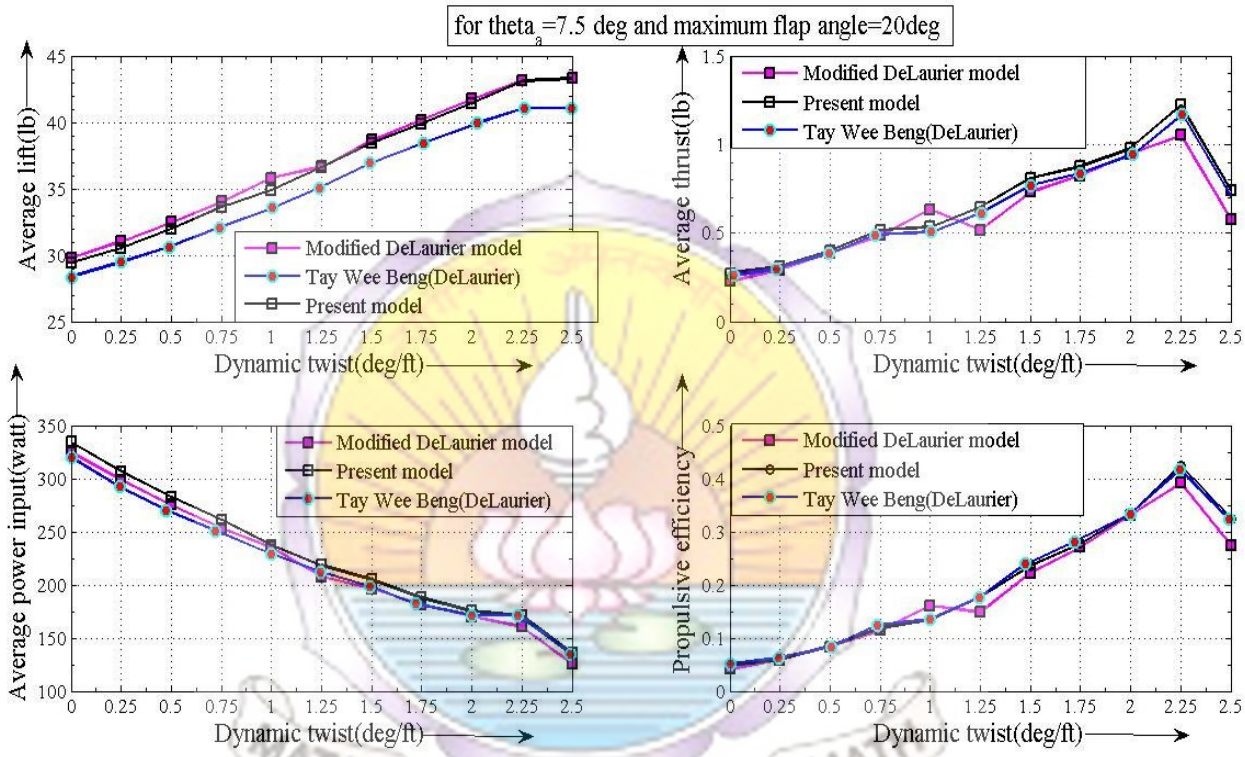

Fig 4.4: Validation of results with literature

4.4 DELAURIER'S MODEL FOR THE AERODYNAMIC PREDICTIONS OF KAVAS

The modified DeLaurier model is applied to KAVAS with the following parameter's being fixed.

- θ_w is assumed to be zero, as the mean angle the chord makes with flapping axis is zero.
- The airfoil was chosen as the Lieback LPT 110A.
- The dynamic stall is not considered. Static stall angle of attack of flap rate is used in the criterion to check whether the flow is attached or detached.

Incorporating all of the above, the aerodynamic prediction of KAVAS is done to obtain the θ_a value for which the lift is greater than the weight, thrust is a positive value and the efficiency is less than one and greater than zero.

Table 5: Aerodynamic parameters using modified DeLaurier model

θ_a(deg)	Velocity (m/s)	β_0(deg/cm)	Lift(N)	Thrust(N)	Power(Watt)	Efficiency
9	2.808	3	0.129	0.2	0.15	0.4

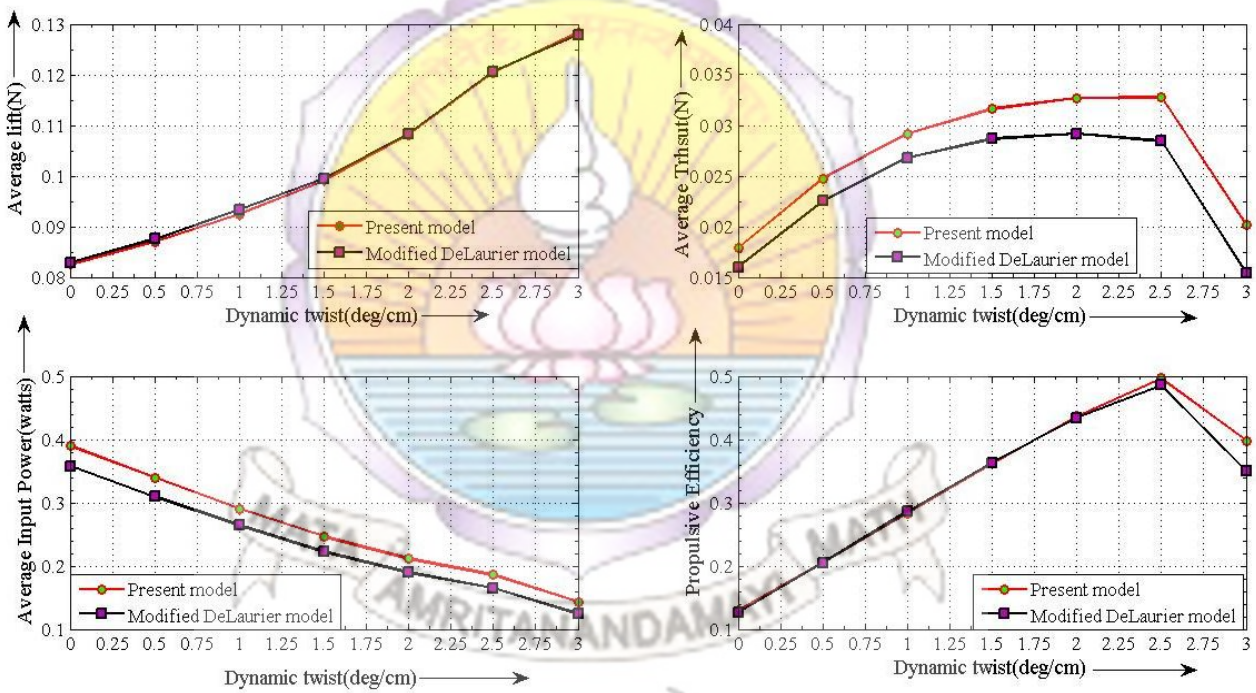

Figure 4.5: Variation of aerodynamic parameters with dynamic twist for KAVAS

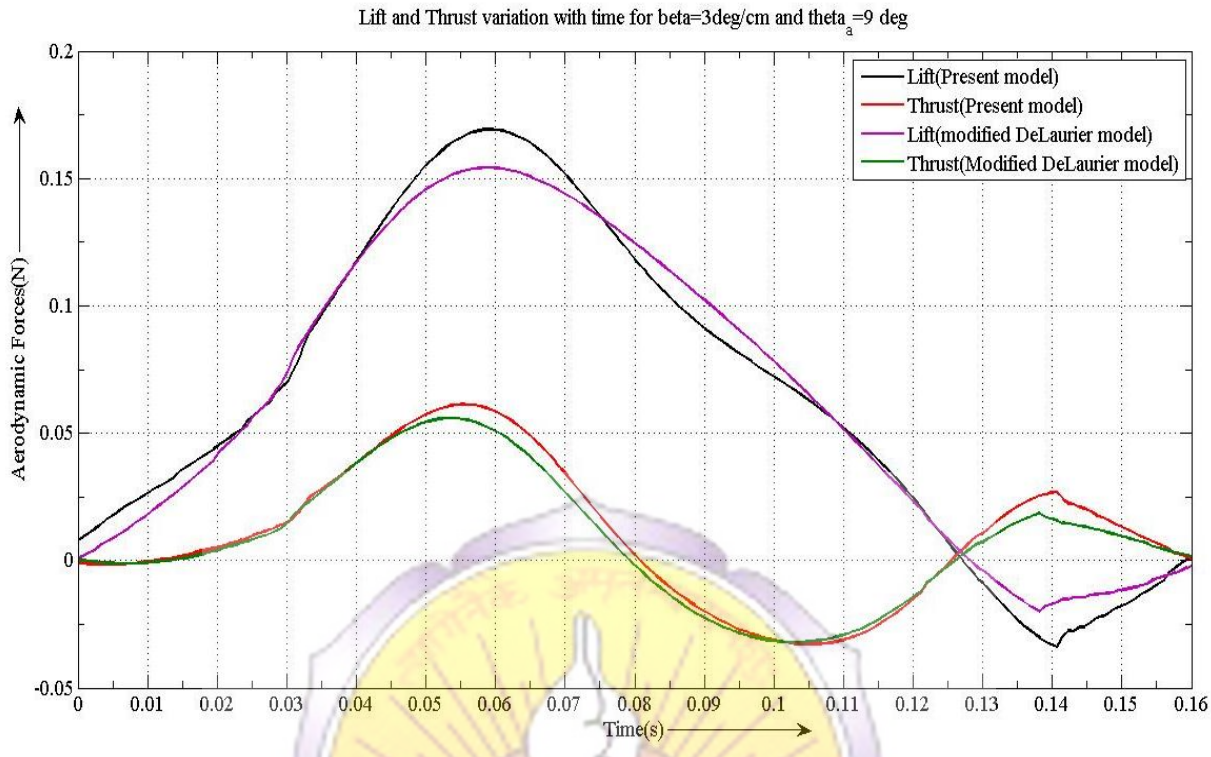

Figure 4.6: Lift and thrust variation with time for KAVAS

CHAPTER 5
CONCLUSION

The project was focussed towards building a flying ornithopter model and analysing it.

- The first few models were unsuccessful due to various issues such as weight of the model, friction encountered in crank mechanism etc. These issues were addressed in a proper fashion and the flying model was fabricated.

- A parametric analysis of the crank mechanism was done to obtain a relation between the crank and flapping angular frequency. This was later refined by determining the flapping frequency of the wing and it was found that only 25% of the input energy was obtained as output.

- An experimental setup was fabricated to select the most suitable rubber band based on angular frequency and it was found that the light rubber band was the best among the 3 types tested as it was consistent.

- The figure of '8' pattern obtained from the LED experiment was due to dynamic twist and provides evidence for material flexibility.

- Through aerodynamic analysis of the ornithopter, the value of β_0 (dynamic twist amplitude) was found to be in the range of 3 deg/cm and the propulsive efficiency was found to lie between 40 to 58%.

- Among the models made with different materials, the napkin model was capable of flying for the longest distance. The fabric model on the other hand was able to fly up to the napkins range, but it was found to have a lower flapping rate than the napkin model. The paper model was the one which covered the least distance. All other models were found to be intermediate between the napkin and the paper model in terms of flapping rate and distance covered.

CHAPTER 6

FUTURE WORK AND REFINEMENT

The following are the suggestions for future work and refinement:

- A more efficient crank mechanism can be designed for better efficiency.
- Different materials can be used for the wing, tail and body and analysed. Other types of rubber bands may also be analysed.
- Different configurations of the model such as biplane, tandem etc. can be fabricated and studied.
- Stiffeners can be inserted between sections of the wings and effects can be observed.
- Different planforms of the wing and tail can be analysed.
- Wing and tail distances may be varied and the effects can be observed.
- Effect of variation of the tail area can be studied.
- A model actuated by other power sources such as electronic motors and actuated by gears can be fabricated to maintain the flapping frequency.
- Hybrid ornithopters can be made using features of RC aircrafts such as micro propellers.

REFERENCES

1. http://en.wikipedia.org/wiki/Ornithopter
2. http://en.wikipedia.org/wiki/Vimana#cite_note-5
3. W., Hudson Shaw and Olaf Ruhen., 1977. "*Lawrence Hargrave: Explorer, Inventor & Aviation Experimenter"*. Cassell Australia Ltd. p. 53.
4. W., Hudson Shaw and Olaf Ruhen., 1977. "*Lawrence Hargrave: Explorer, Inventor & Aviation Experimenter"*. Cassell Australia Ltd. pp. 53–160.
5. Kelly, Maurice., 2006. "*Steam in the Air"*. Ben & Sword Books. Pages 49–55.
6. http://www.ornithopter.org/history.rubber.shtml
7. Bruno Lange, Typenhandbuch der deutschen Luftfahrttechnik, Koblenz, 1986.
8. "Aeroelastic Design and Manufacture of an Efficient Ornithopter Wing" Benedict, Moble. 3–4.
9. http://www.ornithopter.net/history_e.html
10. http://uwmav.uwaterloo.ca/Aeroelastic%20Design%20and%20Manufacture%20of%20an%20Efficient%20Ornithopter%20Wing.pdf
11. http://www.ornithopter.org/history.mav.shtml
12. "Winged robot learns to fly", New Scientist, August 2002.
13. http://www.tudelft.nl/live/pagina.jsp?id=43b123a7-31ac-45a1-a889-4eac9989fd57&lang=en
14. http://www.fai.org/awards/recipient.asp?id=4181
15. http://www.physorg.com/news73578550.html
16. (Article in Dutch newspaper Trouw) http://en.wikipedia.org/wiki/Trouw
17. http://hpo.ornithopter.net/
18. http://www.dailymail.co.uk/sciencetech/article-1370845/SmartBird-mimics-flight-accurately-mistaken-real-thing.html
19. http://www.iitk.ac.in/aero/home/index.php/research/117-flapping-wing-micro-air-vehicle
20. http://orbitalvector.com/Aircraft/Ornithopter/ORNITHOPTER.htm
21. Tanakon Tantanvat, and Sridhar Kota, "Design of Compliant Mechanisms For Minimizing Input Power in Dynamic Applications", Proceedings of IDETC/CIE 2006 ASME 2006 International Design Engineering Technical Conferences & Computers and Informations in Engineering Conference September 10-13,2006 Philadelphia, Pennsylvania, USA.
22. Vance A Tucker, "Gliding Birds: The Effect of Variable Wing Span", Department of Zoology, Duke University, Durham, NC 27706, USA.
23. C. J., Pennycuick, "Control of Gliding Angle in Ruppell's Griffon Vulture Gyps Ruppellii", Department of Zoology, University of Nairobi.
24. C. J., Pennycuick, "Predicting Wing beat Frequency And Wavelength of Birds", Department of Biology, University of Miami, PO Box 249118, Coral Gables, FL 33124, USA.
25. B. G., Newman, "Soaring And Gliding Flight of the Black Vulture", Department of Engineering, University of Cambridge.
26. Karl Axel Strang, "Efficient Flapping Flight of Pterosaurs", Department of Aeronautics and Astronautics, Stanford University.
27. Vance A., Tucker, and G., Christian Parrott, "Aerodynamics of Gliding Flight In a Falcon and Other Birds" Department of Zoology, Duke University, Durham, North Carolina.

28. Chao Wang, Chaiying Zhou, Xingwei Zhang, Cong Liu "An Optimization on Single-Crank-Double-Rocker Flapping Wing Mechanism", Department of Mechanical Engineering and Automation, Shenzhen Graduate School, Harbin Institute of Technology, Xili Shenzhen University Town, Shenzhen 518055, China.
29. Thomas J., Mueller, and James D., DeLaurier, "Aerodynamics of Small Vehicles", Annu. Rev. Fluid Mech.2003.
30. Theodore Yaotsu Wu, "Fish Swimming and Bird/Insect Flight", Engineering and Applied Science, California Institute of Technology, Pasadena, California.
31. Jerke Eisma, "Flow Visualization and Force Measurements on a Flapping Wing MAV Delfly II in Forward Flight Configuration", Delft university of Technology.
32. T., Nick, Pornsin-Sirirak, Yu-Chong Tai, Chih-Ming Ho, Matt Keennon, "Microbat: A Palm-Sized Electrically Powered Ornithopter", Electrical Engineering, California Institute of Technology, Pasadena, USA.
33. Lan Liu, Zongde Fang and Zhaoxiz He "Optimization Design of Flapping Mechanism and Wings for Flapping-Wing MAVs", School of mechatronics, Northwestern Polytechnical University, Xi'an, China.
34. Dmytro Silin, "Aerodynamics And Flight Performance of Flapping Wing Micro Air Vehicles", University of Arizona.
35. Mark Ryan, "Design Optimization And Classification of Compliant Mechanisms For Flapping Wing Micro Air Vehicles", The Ohio State University.
36. Harijono Djojodihardjoa, Alif Syamim Syazwan Ramli and Surjatin Wiriadidjaja "Kinematic and Aerodynamic Modelling of Flapping Wing Ornithopter", International Conference on Advanced Science and Contemporary Engineering 2012.
37. J., D., DeLaurier, "An Aerodynamic Model For Flapping Wing Flight", Institute of Aerospace Studies, University of Toronto, Downsview, Ontario, Canada.
38. G., C., H., E., de Croon, K., M., E., de Clercq, R., Ruijsink, B., Remes, and C., de Wagter, "Design, Aerodynamics and Vision Based Control of the Delfly.
39. Lung-Jieh Yang, Cheng Kuei Hsu, Fu-Yuan Hsiao, Chao-Kung Feng and Yung-Kang Shen "A Micro-Aerial-Vehicle (MAV) With Figure-of-Eight Flapping Induced by Flexible Wing Frames".
40. "Dynamics and Control of a Flapping Wing Aircraft" by Tay Wee Beng.
41. http://www.instructables.com/id/Ornithopter/
42. "Building an Ornithopter" by William Gurstelle.
43. http://birdkit.com/tips.html
44. http://www.toktol.com/notes/context/physics/sinusoidal-oscillations/relationship-between-angular-frequency-and-angular-velocity
45. Prouty, R.W., Airfoils for rotor blades, Helicopter Performance, Stability, and Control, PWS Engineering Boston, 1986, pp 397-409.
46. Shyy, W., Kamakoti, R., Berg, M., and Ljungqvist, D., A computational study for biological flapping wing flight. *Trans Aeronautical and Astronautical Society* 32(4): pp 265-279. 2000

APPENDIX A-1

MATLAB CODE FOR AERODYNAMIC PERFORMANCE PREDICTION OF ORNITHOPTER

```
clc
clear all
format short
alphastall=13*pi/180;
Cmac=0.025;
aspectratio=4.7;
alpha_o=0.5*pi/180;
gamma=33.5*pi/180;                                  % maximum flapping
angle(rad)
eta=0.98;                                           % leading edge suction efficiency
rho=1.23;                                           % density of air(kg/m^3)
theta_a=9*pi/180;                                   % pitching angle of flapping angle
with respect to U(rad)
f=6.15;                                             % flapping frequency (Hz)
U=2.8;                                              % forward velocity (m/s)
mew=1.46e-5;                                        % (coefficient of viscocity(kg/ms))
dt=1/(20*f); %time interval
dy=0.01;%section width
ddy=dy*100;
beta=0:0.25:2.5;
for z=1:length(beta)
theta_o=beta(z)*1*pi/180;                           % pitching motion
amplitude(rad/m)
%     beta(z+1)=zz(z)*1;
for x = 0:ddy:20
num=(x/ddy)+1;
c(num) = (- 0.036*x^2 + 0.13*x + 12)*0.01;
o=(pi*f*c(num)/U);                                  % reduced frequency
count=1;
for t = 0:dt:1/f
dihedral=gamma*cos(2*pi*f*t);
theta=-theta_o*(x+(9/2))*sin(2*pi*f*t)+theta_a;
h=-gamma*(x+(9/2))*cos(2*pi*f*t);
hdot=gamma*(x+(9/2))*sin(2*pi*f*t)*2*pi*f;
hdoubledot=-((2*pi*f)^2)*h;
thetadot=-theta_o*(x+(9/2))*cos(2*pi*f*t)*2*pi*f;
thetadoubledot=theta_o*(x+(9/2))*sin(2*pi*f*t)*2*pi*f*2*pi*f;
Vpitch=0.75*c(num)*thetadot;
Vplunge=hdot*cos(theta-theta_a);
Downwardvelocity=U*(theta-theta_a);
Vpitchdot=0.75*c(num)*thetadoubledot;
Vplungedot=-hdot*sin(theta-theta_a)*thetadot+hdoubledot*cos(theta-theta_a);
Downwardvelocitydot=U*thetadot;
temp(num,count)=(Vpitch+Vplunge+Downwardvelocity)/U;
```

```
alpha=((temp(num,count)));
angle(num,count)=((Vpitchdot+Vplungedot+Downwardvelocitydot)/U)*180/pi;
alphadot=(Vpitchdot+Vplungedot+Downwardvelocitydot)/U;
AR=aspectratio;
C1=0.5*AR/(2.32+AR);
C2=0.181+(0.772/AR);
F=1-(C1*o*o/(o*o+C2^2));
G=-(C1*C2*o)/(o*o+C2^2);
C=(F*F+G*G)^0.5;
w=U*2*(alpha_o+theta_a)/(2+AR);
alphap=((AR/(2+AR))*(F*alpha+(c(num)/(2*U))*(G/o)*alphadot))-w/U;
b=U*alphadot-0.25*c(num)*thetadoubledot;
Vx=U*cos(theta)-hdot*sin(theta-theta_a);
%               velocityx(num,count)=U*cos(theta)-hdot*sin(theta-theta_a);
tempp(num,count)=((alphap+theta_a-(0.75*c(num)*thetadot/U)))*180/pi;
if (alphap+theta_a-((0.75*c(num)*thetadot)/U)) >= alphastall
Vn=hdot*cos(theta-theta_a)+0.5*c(num)*thetadot+U*sin(theta);
Vs=sqrt((Vx*Vx+Vn*Vn));
dNc(num,count)=1.98*Vs*Vn*c(num)*rho*dy/2;
dNa(num,count)=rho*pi*c(num)*c(num)*(b/8)*dy;
dDf(num,count)=0;
dTs(num,count)=0;
dDcamb(num,count)=0;
dPin(num,count)=(dNc(num,count)+dNa(num,count))*(hdot*cos(theta-
theta_a)+0.5*c(num)*thetadot);
dL(num,count)=((dNa(num,count)+dNc(num,count))*cos(theta)+(dTs(num,count)-
dDf(num,count)-dDcamb(num,count))*sin(theta))*cos(dihedral);
dT(num,count)=          (dTs(num,count)-dDf(num,count)-dDcamb(num,count))*cos(theta)-
(dNa(num,count)+dNc(num,count))*sin(theta);
else
Vy=U*(alphap+theta_a)-0.5*c(num)*thetadot;
%               velocityy(num,count)=U*(alphap+theta_a)-0.5*c(num)*thetadot;
V=sqrt((Vx)^2+(Vy)^2);
dDcamb(num,count)=-2*pi*alpha_o*(alphap+theta_a)*rho*U*V*c(num)*dy*0.5;
dNc(num,count)=rho*U*V*pi*(alphap+theta_a+alpha_o                    )*dy*c(num);
%circulatory normal force
dNa(num,count)=rho*pi*c(num)*c(num)*b/4*dy;
%normal force due to apparent mass effect
dTs(num,count)=eta*2*pi*(alphap+theta_a-
((0.25*c(num)*thetadot)/U))^2*rho*U*(V/2).*dy*c(num);      %leading edge suction force
re=U*c(num)/(mew);
Cdp(num,count)=0.89*(log10(re))^-2.58;
dDf(num,count)=Cdp(num,count)*rho*(Vx)^2*c(num)*dy*0.5;                    %
friction drag
dFx=(dTs(num,count)-dDcamb(num,count)-dDf(num,count));
dN=((dNa(num,count)+dNc(num,count)));
dL(num,count)=(dN*cos(theta)+dFx*sin(theta))*cos(dihedral);
dT(num,count)= dFx*cos(theta)-dN*sin(theta);
```

```
dM=-
((rho*pi*c(num).*c(num).*c(num)*thetadot*U/16)+(rho*pi*c(num).*c(num).*c(num)*c(nu
m)*thetadoubledot)/128)*dy;
dmac=Cmac*rho*dy*(c(num).^2)*U*V*0.5;
dPin(num,count)=((dTs(num,count)-dDf(num,count)-dDcamb(num,count))*hdot*sin(theta-
theta_a))+((dNa(num,count)+dNc(num,count))*(hdot*cos(theta-
theta_a)+0.25*c(num)*thetadot))+(0.25*c(num)*thetadot*dNa(num,count))-
(dM+dmac)*thetadot;
end
time(count)=t;
count=count+1;
end
end
avglift=0;
avgthrust=0;
avgpower=0;
for i=1:count-1
lift(i)=0;
thrust(i)=0;
power(i)=0;
end
for i=1:count-1
for k=1:num
lift(i)=lift(i)+dL(k,i);
thrust(i)=thrust(i)+dT(k,i);
power(i)=power(i)+dPin(k,i);
end
avglift=avglift+lift(i)*dt;
avgthrust=avgthrust+thrust(i)*dt;
avgpower=avgpower+power(i)*dt;
end
avgliftt(z)=avglift*f;
avgthrustt(z)=avgthrust*f;
averagepowerinput(z)=avgpower*f;
efficiency(z)=(avgthrustt(z)*U)/averagepowerinput(z);
end
% plot(time,lift,time,thrust)
% plot(beta,avgthrustt)
[LX,A1,A2]= plotyy(beta,2*averagepowerinput,beta,efficiency,'plot')
set(get(LX(1),'Ylabel'),'String','Avg Input Power(watt)')
set(get(LX(2),'Ylabel'),'String','Propulsive Efficiency')
figure (2)
[AX,H1,H2] = plotyy(beta,2*avgliftt,beta,2*avgthrustt,'plot')
set(get(AX(1),'Ylabel'),'String','Avg Lift(N)')
set(get(AX(2),'Ylabel'),'String','Avg Thrust(N)')
```

APPENDIX A-2

PROCEDURE TO OBTAIN VELOCITY TRIANGLE

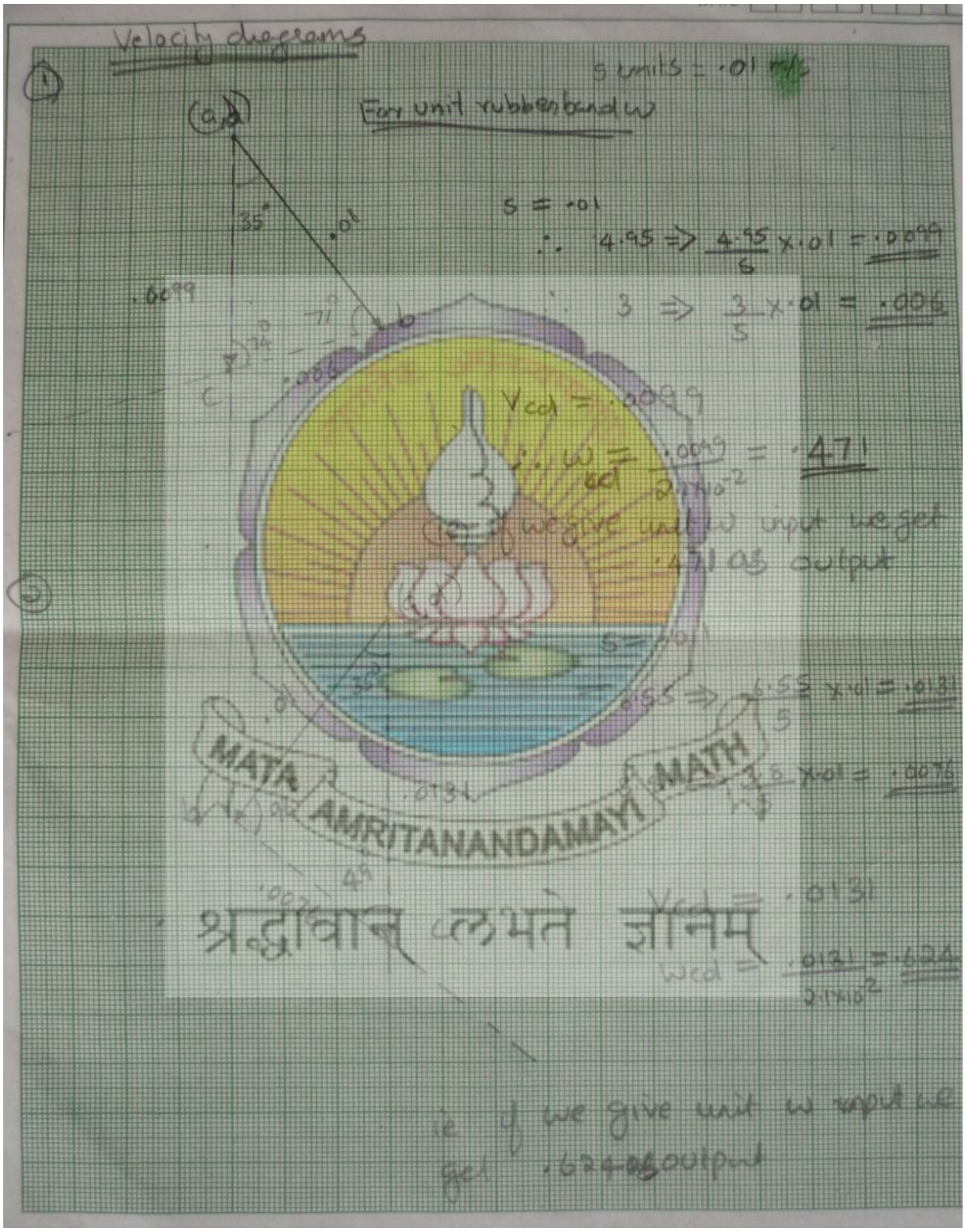


5 units = ·815 m/s
Vab = ·82
wab = ·82 / 1 = 82
Vdb = ·617
wdb = ·617 / 1 = 617
MATA AMRITANANDAMAYI MATH
श्रद्धावान् लभते ज्ञानम्